Pergamon

www.elsevier.com/locate/jappmathmech

PII: S0021-8928(03)00119-9

*J. Appl. Maths Mechs*, Vol. 67, No. 5, pp. 703–730, 2003

0021-8928/$—see front matter

# AXISYMMETRIC NOSE SHAPES OF SPECIFIED ASPECT RATIO, OPTIMUM OR CLOSE TO OPTIMUM WITH RESPECT TO WAVE DRAG†

A. N. KRAIKO, D. Ye PUDOVIKOV,
K. S. P'YANKOV and N. I. TILLYAYEVA

Moscow

e-mail: akraiko@ciam.ru

(*Received* 25 *March* 2003)

The problem of constructing optimum or close to optimum nose-shapes of bodies of revolution of fixed aspect ratio in a supersonic flow is solved within the framework of a perfect (inviscid and non-heat-conducting) gas. Their contour includes the front face, that is, the boundary extremum section with respect to the length and, adjacent to it, the smooth, slightly sloping section that makes a corner. In case of low aspect ratios, the slightly sloping section is the result of the exact solution of a variational problem. In the case of aspect ratios which exceed a certain value, depending on the free-stream Mach number $M_\infty$, the exact solution requires the introduction of small internal breaks with corner points where even the dominant one of these only has a weak effect on the drag value. Contours which are referred to as "close to optimum" do not satisfy the optimality condition, which defines the dominant corner. In the examples ($1.2 \le M_\infty \le 10$) for which calculations were carried out, conical nose shapes were found to be far worse that the optimum ones. For contours which are optimum in the approximation of Newton's formula and also, optimum blunt and pointed, power-law nose shapes, the situation occurs for low-aspect ratios and low supersonic Mach numbers (pointed, power-law contours can only be successfully constructed for fairly high aspect ratios). The fact that the front face is a section of a boundary extremum is shown by comparing the drags of bodies obtained with different permissible variations of the front face. An alternative proof, which is not limited by the actual form of the variation in the front face, can be obtained from the solution of the conjugate problem, formulated within the framework of the general method of Lagrange multipliers. This problem is also of interest in its own right, in particular, on account of the singularities, revealed during its formulation, in the reflection of the discontinuities of the Lagrange multipliers from the sonic line with parts of them becoming infinite at the point of reflect. 

## 1. INTRODUCTION

The problem of constructing an axisymmetric nose shape with a specified aspect ratio which has minimum drag, that is, "Newton's problem", was solved by Newton at the dawn of the calculus of variations using formula he proposed for determining the pressure $p$ on the body surface (Newton's formula)

$$p = p_\infty + \rho_\infty V_\infty^2 \sin^2 \vartheta \tag{1.1}$$

Here, $\rho$ is the density, $V$ is the modulus of the velocity $\mathbf{V}$, free stream parameters are indicated with the subscript $\infty$, and $\vartheta$ is the angle between the tangent to the contour and $\mathbf{V}_\infty$.

For a long time, Newton's solution [1] was considered without reference to aerodynamics but, at the beginning of the 1950's, it was ascertained that Newton's formula works quite well at hypersonic speeds. At the same time, aerodynamicists turned to the construction of optimum and, in the first place, of planar and axisymmetric bodies using Newton's formula (1.1). Until that time, Newton's solution, which was well known to mathematicians, was not, as a rule, known to aerodynamicists who were occupied with solving Newton's problem and different generalizations of it. Moreover, even the description in the "Mathematical Origins of Natural Philosophy", which is closest to the modern method of obtaining it given in the remarks of Krylov [1], turned out to be rather difficult for aerodynamicists of that time to understand. Western specialists appeared to be in an even more difficult position. The above-mentioned remarks were unavailable to them, and the description of this method of solution discussed in [2] and found in Newton's correspondence was far more difficult to understand from contemporary positions. The absence of references to Newton's solution in many of the "first" papers dealing with this question is apparently explained by this. But when, nevertheless, this was remembered, as was done by Egger *et al.* [3, 4], the front face, an obligatory element of Newton's solution, was introduced without explanation and, as was subsequently revealed [5], without understanding the reasons for its appearance.

†*Prikl. Mat. Mekh.* Vol. 67, No. 5, pp. 795–828, 2003.

The first attempt to solve Newton's problem using the more complex Newton–Busemann formula and, as then represented, more accurate formula than (1.1), was made in [6]. Two problems arose in connection with the extremal generatrices found in [6] using this formula which satisfy the classical condition for an extremum ("Euler's equation" of the calculus of variations). First, as in the case of Newton's formula, the extremals, as a rule (the exceptions, which are not of special interest, are a front face, that is, a body of zero aspect ration, and a needle, a body of infinite aspect ratio) could not originate on the axis of symmetry, that is, they were the generatrices of bodies with a channel. Second, the replacement of a non-zero angle of inclination of the extremal at its end point with zero reduced the drag by a finite amount. The possibility of such a reduction is associated with the fact that, according to the Newton–Busemann equation, in the case of flow past convex corners the pressure at a corner point becomes minus infinity, leading to a finite "thrust effect" which reduces the drag. In a gas $p \geq 0$, and this effect is a consequence of the incompleteness of the Newton–Busemann equation, which must be taken into account when formulating the variational problem. It was established in [7] that taking account of this leads to the fact that, within the framework of the Newton–Busemann equation, the terminal section of the optimum nose shape turns out to be a section of the boundary extremum, that is, the limit of applicability of Newton–Busemann equation which is defined by the equality $p = 0$.

The impossibility of drawing the required two-sided extremum from the axis of symmetry leads to the introduction of another section of the boundary extremum [1, 2, 8–11]. The front face, which is present in Newton's solution, is such section. In the Newtonian case, the front face is a section of the boundary extremal, which appears on account of the constraint on the length of the nose section. For this reason, only non-negative variations of the longitudinal coordinate $\delta x \geq 0$ are permissible on the front face. However, as Legendre noted, when it is assumed at the front face $\delta x > 0$ the drag of the nose section constructed by Newton can be reduced, albeit not in the first order but in the second order with respect to $\delta x' \equiv d\delta x/dy$, as a front face, satisfying the necessary bilateral extremum condition, does not satisfy Legendre's condition, which is a necessary condition for a "weak" minimum. By virtue of this last condition, extremals which realize a minimum in the drag must satisfy the inequality $dx/dy \equiv \operatorname{ctg}\vartheta \geq \dfrac{1}{\sqrt{3}}$, where $y$ is the radial coordinate of the cylindrical coordinates $x$ and $y$.

In spite of Legendre's observation, Newton's solution with a front face is correct, since the front face is a section of the boundary extremum not only on account of the constraint on the length of the nose shapes but also as the limit of applicability of Newton's equation. In the case of nose shapes, this formula holds if $0 \leq \vartheta \leq \pi/2$, and the front face turns out to be simultaneously a section of the boundary extremum with respect to both $x$ and $\vartheta$. In fact, Newton, who did not know the Legendre condition, not only showed that, in the light of the above-mentioned constraints, the front face is such a section but also obtained the necessary condition (see [1, pp. 428–433]) for the optimality of a bilateral extremal: $dx/dy \geq 1$ which is stronger than the Legendre condition. Legendre did not note this Newtonian inequality.

The section $p = 0$, when the Newton–busemann equation is used, and the front face when the length is specified do not exhaust all sections of the boundary extremum in problems of constructing axisymmetric (and planar) nose shapes of minimum wave drag. In the case of a free length, another type of section of the boundary extremum appears when constructing planar and axisymmetric nose shapes of specified volume within the framework of Newton's formula [5, 11]. Here, in the case of small and moderate values of the dimensionless volume, nose shapes of minimum wave drag have the form of a pin which protrudes from the front face of the given body. According to results obtained earlier [5, 11], the above-mentioned inequality $dx/dy \geq 1$ must be satisfied in the sections of the bilateral extremum in the problem with a specified volume (in the case of a free length) solved using Newton's equation (1.1) and in Newton's problem.

The attention paid above to the construction of optimum nose shapes within the framework of Newton's formula and the Newton–Busemann formula is also justified when the same problem is considered within the framework of the full equations for the flow of an inviscid and non-heat-conducting gas ("Euler's equations"). In the first place, the value of the results discussed above is due to the fact that the same problem, i.e. that there are no sharp-pointed, extremal generatrices differing from a needle, around which there is a flow with an attached bow shock wave, arises when constructing axisymmetric nose shapes of minimum wave drag in the approximation of Euler's equations. This problem, as when Newton and the Newton–Busemann equations are used, does not arise in the case of sufficiently long nose shapes. However, another problem, associated with the corner points of the optimum generatrix does arise. The contribution of these corner points to the drag of optimum planar nose shapes is known with a high degree of completeness. The results obtained in the approximation of Euler's equations for optimum planar nose shapes are also important when constructing their axisymmetric analogues.

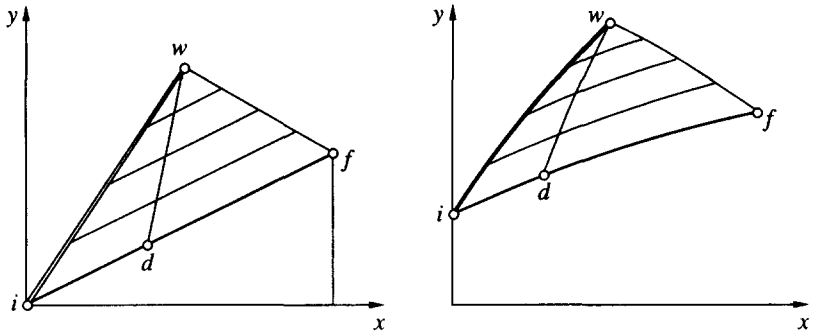


Fig. 1

Within the framework of Euler's equations, the first exact result concerning the constructing of a planar nose shape of specified aspect ration, which gives minimum wave drag in a supersonic flow of a perfect gas, was obtained by Chernyi [12]. On investigating the flow close to wedge-shaped bodies, he picked out the cases when a wedge is an optimum nose shape and established that this is possible when the reflection coefficient for the shock wave of pressure perturbations arriving at it along the $C+$-characteristics, vanishes (see Fig. 1, where *if* is the generatrix of the nose shape, *iw* is the attached shock wave, and *dw* and *wf* are the $C^+$- and $C^-$-characteristics). For each fixed free stream, this condition is satisfied only for wedges of certain aspect ratios $l = x_f/y_f$, including a wedge of infinite aspect ratio with a zero angle at the vertex and a shock wave which has degenerated into the $C^+$-characteristic. Later, the same result was independently obtained by Shmyglevskii, by whom the corresponding variational problem was solved using Euler's equations.

The above-mentioned problem was solved in [13] using a control contour consisting of the shock wave *iw* and the "closing" $C^-$-characteristic *wf*. The schemes for the supersonic flow past a wedge with an attached bow shock wave and the nose section of a body of revolution with a channel are shown on the left and the right of Fig. 1 respectively. In the control contour method, the drag of the generatrix *if* is expressed, using the integral law of conservation of the axial component of linear momentum, in terms of integrals with respect to the sections *iw* and *wf*. The specified length of the nose section and the equality of the flow rates across *iw* and *wf* are expressed as the difference of the integrals along them. The entropy of the gas behind the shock wave, which is subsequently conserved along the streamlines, is a known function of its angle of inclination $\sigma$ to the $x$ axis and, along the closing $C^-$-characteristic, the parameters (including $x$, $y$ and the stream function $\psi$) are related by the ordinary differential equations. When account is taken of this in the control contour method, the variational problem of determining the optimum generatrix *if* reduces to a Lagrangian problem with isoperimetric conditions and with additional relations in the form of ordinary differential equations. The necessary conditions for an extremum give the equations for the optimum shape of the section *iw* of the shock wave, that is, the function $\sigma = \sigma(\psi)$ and the optimum distributions of the parameters on the section *wf* of the extreme $C^-$-characteristic. If the above-mentioned sections and the parameters in them are known, the problem of finding the contour *if* corresponding to them reduces to the numerical solution of two standard problems by the method of characteristics: a Cauchy problem with data on the shock wave section *iw* and a Gourset problem with data on the sections *dw* and *wf* of the characteristics of the different families. An analysis of the necessary conditions for an extremum obtained by Shmyglevskii [13] showed that they can only be satisfied for the same aspect ratios $l$ of a planar nose shapes, as were indicated by Chernyi [12]. In the case of a perfect gas with a constant ratio of the heat capacities $\kappa$, the number of such aspect ratios, besides $l = \infty$, varies from one to three [10–14] depending on the free-stream Mach number $1 < M_\infty \leq \infty$.

In the case of nose shapes of bodies of revolution, analogous results were obtained using the control contour method [14–16]. The results in [13–16] were extended in [17] to an arbitrary two-parameter gas. According to [14–17], an optimum bow shock wave, differing from the $C^+$-characteristic, cannot start from the axis of symmetry. Hence, the optimum smooth contours *if*, differing from a needle, found in [14–17] by the control contour method, can only be considered as the generatrices of nose shapes of bodies of revolution with a channel (also, see [10, 18]. This situation is analogous to that which occurred when constructing the optimum, axisymmetric nose shapes using Newton's equation and the Newton–Busemann equation.

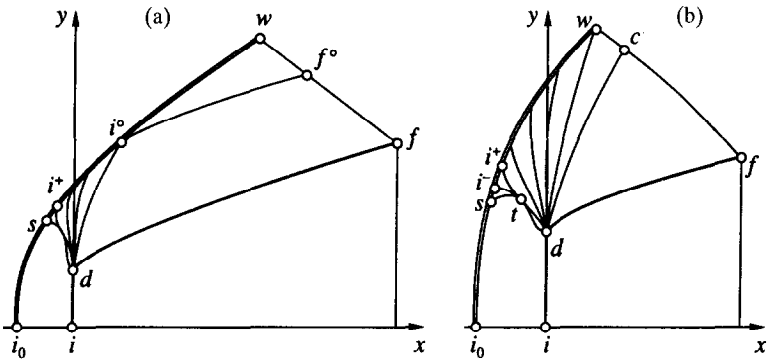


Fig. 2

Optimality conditions, which, in the axisymmetric case, determine the extremal sections of the shock wave and the closing $C^+$-characteristic, are required later. In the case of a two-parameter gas, they have the form [11, 16]

$$\frac{\mu^\circ}{\mu}\frac{y\rho v^2}{(y\rho u)_\infty} + \frac{T v_s (u_s - u_\infty)}{T_s V^2}[(1+\Omega M^2)v + u\sqrt{M^2-1}] = 0 \tag{1.2}$$

$$y\rho V^2 \sin^2\vartheta \operatorname{tg}\alpha = -\mu = \text{const} \tag{1.3}$$

Here, $M = V/a$ is the Mach number, $a$ is the speed of sound, $u$ and $v$ are the $x$ and $y$ components of the velocity $\mathbf{V}$, $\alpha$ is the Mach angle: $\operatorname{ctg}\alpha = (M^2-1)^{1/2}$, $T$ is the temperature, $\Omega = -a^2/(\rho i_\rho)$ and $i_\rho = (\partial i/\partial\rho)_p$, where $i = i(p, \rho)$ is the specific enthalpy, a known function of $p$ and $\rho$. For a perfect gas, $\Omega = \kappa - 1$, the parameters on the $C^-$-characteristic $wf$ without subscripts and the parameters behind the shock wave (with the subscript $s$) correspond to the same values of $\psi, y_\infty \equiv y_\infty(\psi) = [2\psi/(k\rho_\infty V_\infty)]^{1/2}$ with an arbitrary normalizing factor $k > 0$, and $\mu^\circ$ and $\mu$ are constants. In the cases considered in [10, 13–18], $\mu^\circ = \mu$. In this case, by virtue of equality (1.3) which holds, in particular, at the point $w$ in it

$$\Lambda_w \sim \lambda_w \equiv v_w\left\{\rho v + \frac{\rho_\infty u_\infty (u - u_\infty)}{V^2}[(1+\Omega M^2)v + u\sqrt{M^2-1}]\right\}_w = 0 \tag{1.4}$$

which is equivalent to the above-mentioned reflection coefficient $\Lambda_w$ vanishing. For specified coordinates of the terminal points belonging to the bow shock wave and the closing $C^-$-characteristic, any of the streamlines sketched in Fig. 1 are optimum generatrices. Equality (1.3) with $\mu^\circ/\mu \neq 1$ will be discussed later.

It has been proposed that the particular class of smooth, axisymmetric contours of minimum wave drag, found in [14, 15], should be used [15, 19] to construct axisymmetric nose shapes of bodies without a channel which give minimum wave drag for a specified initial section $id$. Specification of the section $id$ under the assumption that there is a corner at point $d$ uniquely defines the flow (including the shock wave $i_0 i^\circ$) to the left of $di^\circ$, that is, to the left of the closing $C^+$-characteristic of the bunch of rarefaction waves which arise in the flow about the corner point $d$. The section $id$ could, as in Fig. 2(a) be specified in the form of a front face: $x = 0$. However, actual examples were not constructed in [15, 19]. For bodies of the type considered in [15, 19] the angle of inclination of the shock wave at the point $i^\circ$ is such that a section of the wave $i^\circ w$ and an "extremal" triangular domain $i^\circ wf^\circ$ can be continuously added to the shock wave $i_0 i^\circ$ in it. The sections $i^\circ w$ and $wf^\circ$ of the shock wave and the $C^-$-characteristic satisfy conditions (1.2) and (1.3) with $\mu^\circ = \mu$, and with $i$ and $f$ replaced by $i^\circ$ and $f^\circ$. The section $f^\circ f$ of the closing $C^-$-characteristic is found using the optimally condition (1.3) for a known entropy, that is determined by the initial section of the shock wave $i_0 i^\circ$, which is independent of the shape of the contour $df$.

Within the framework of Newton's equation and the Newton–Busemann equation, optimum planar nose shapes can be constructed for any aspect ratios greater than unity (as well as the nose shapes of bodies of revolution with a channel over a certain range of aspect ratios and relative radii of the channel).

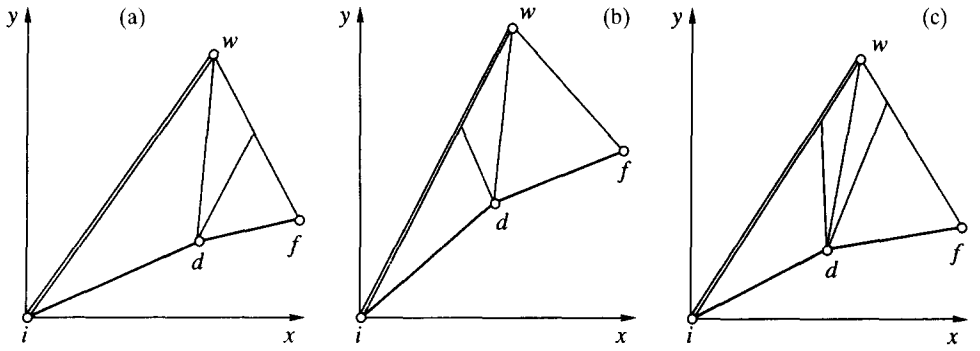


Fig. 3

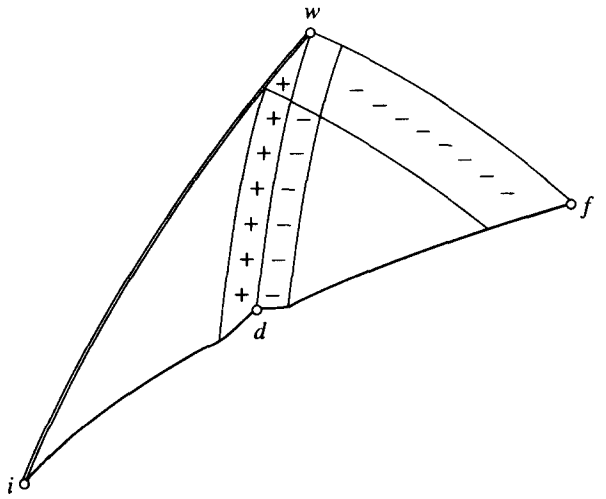


Fig. 4

In connection with the results in [12–19], the question therefore arises as to why it is not possible to do this when solving the same problems within the framework of Euler's equations. An analysis of the possible limitation of the control contour method, used in [13–18], provides an answer to this. The point is that the possibility of an independent and sign-variable variation of the angle of inclination of the shock wave $\sigma$ and $p$ or $\vartheta$ in the closing $C^-$-characteristic is implicitly assumed when obtaining the required optimality conditions by this method. In the case of smooth bodies, this is in fact so since the initial section of the contour *id* defines the form of the shock wave, and its final section *df* defines the closing characteristic. If, however, the optimum contour has a corner point, the possibility of either a sign-variable (Fig. 3a and b) or a sign-variable and independent (Fig. 3c) variation in the sections of the shock wave and the closing characteristic falling into the bunch of rarefaction waves disappears.

The fact that, within the framework of Euler's equations, the optimum contour cannot be smooth in the general case is proved using the technique of variation in a characteristic "ε-band", proposed in [12] (Fig. 4). Suppose the optimum generatrix *if* is smooth and that, for example, the coefficient $\Lambda_w$ is negative. We now only vary the inclination of the contour in the ε-neighbourhood of point $d$ by $\Delta > 0$ to the left of point $d$ and by $-\Delta$ to the right of it. Then, for small ε and Δ, the perturbations of the parameters are described by the solution of Euler's equations with reference, in the general case, to uniform unperturbed flow (which corresponds to $\Delta = 0$). The perturbations of the parameters will be quantities of the order of Δ only in the characteristic bands going to the shock wave and in the reflected characteristic band shown in Fig. 4, where the + and – signs indicate positive and negative variations $\delta p = O(\Delta)$. Only the left half of the ε-band with $\delta p = O(\Delta) < 0$ falls within the neighbourhood of the point $f$ on the nose shape contour, which leads to a reduction in the drag by $O(\varepsilon\Delta)$ while the contribution of the remaining sections of the contour is equal to $O(\varepsilon^2\Delta)$. If $\Lambda_w > 0$, the same result is obtained when the protuberance in the neighbourhood of point $d$ is replaced by an indentation. The possibility of a reduction in the drag contradicts the supposition of the optimality of the smooth contour. When there

is a break of finite angle at point $d$, the contribution to the drag from its varied neighbourhood is found to be a quantity of the order of $\varepsilon\Delta$, and such a contradiction does not arise.

So, in the general case of a non-zero reflection coefficient $\Lambda_w$, the optimum contour cannot be smooth. Moreover, it can be shown by the same technique [10] that, within the framework of Euler's equations, optimum contours in a flow with attached shock wave do not, in general, have just one but infinitely many corner points and points of their condensation. Such as at first glance, hopeless situation (in the sense of the construction of the optimum solution) is simplified due to the fact that the break angle at the dominant corner point is proportional to $\Lambda$, the angle at the following corner point is proportional to $\Lambda^2$ and so on when, as a rule, $|\Lambda| \ll 1$. The introduction of just a single corner point therefore enables one to obtain the main and exceedingly small reduction in the wave drag.

The first, close to optimum, contours with a single corner point in a flow with an attached shock wave were constructed in [20, 21] using an extremely complicated numerical algorithm, which includes the method of characteristics and the optimality conditions obtained within the general framework of the method of Lagrange multipliers [10]. 21 generatrices with a single corner point were constructed in [20, 21]: 7 nose profiles and 14 shells of bodies of revolution with a channel. All of the planar generatrices, constructed for a flow of a perfect gas with $\kappa = 1.4$ past them, had a corner point with the break angle that did not exceed 0.05 with a maximum reduction in the wave drag of 0.66% compared with a wedge. The drag of the generatrices of the nose shapes of bodies of revolution with a channel, when compared with smooth rectilinear generatrices with the same coordinates of the points *i and* f, turned out to be several percent lower. However, this last fact is not due to the existence of the corner point but to the fact that, in the axisymmetric case, rectilinear generatrices are also not optimum when $\Lambda_w = 0$ and, when $\Lambda_w = 0$, their drag exceeds the drags of generatrices, the shape of which is defined by conditions (1.2) and (1.3) with $\mu^\circ/\mu = 1$, by the same percentages.

A method of constructing close to optimum smooth generatrices of bodies of revolution with a channel has been developed in [22] within the framework of the method of indefinite control contour [10]. Here (also, see [11]), after conditions (1.2) and (1.3) with $\mu^\circ/\mu \neq 1$, which must be satisfied on the shock wave *iw* and on the characteristic *wf*, have been obtained, the single term

$$\delta\chi = (\mu^\circ - \mu)\delta x_w = y_w\lambda_w(M_w^2 - 1)^{-1/2}\delta x_w \tag{1.5}$$

remains in the expression for the variation of the wave drag $\delta\chi$, where $\delta x_w$ is the increment in $x_w$ for fixed $y_w$ and $\psi_w$. In the case of arbitrary non-zero variations $\delta x_w$, the right-hand side of equality (1.5) is equal to zero only when the coefficient $\Lambda_w$, which is defined by by formula (1.4), is equal to zero. This gives the smooth optimum generatrices investigated in [14–18]. When $\Lambda_w \neq 0$, equalities (1.2) and (1.3), written at the point $w$, determine the constants $\mu$ and $\mu^\circ/\mu \neq 1$. The use of the same parameters with the $\mu$ and $\mu^\circ/\mu$, which have been found when $\psi < \psi_w$, enables one to construct the corresponding sections of the shock wave and the closing $C^-$-characteristic and, using these, also the continuum of smooth, close to optimum generatrices. They are "close to optimum" on account of the smallness of $\Lambda_w$ mentioned above and not optimum on account of the existence of a non-zero right-hand side of (1.5). Comparisons carried out confirmed the closeness of the smooth contours obtained by this method to almost optimum contours with a single corner point. The wave drag coefficients of nine out of the fourteen generatrices with a corner point constructed in [20, 21] and of the smooth generatrices constructed in [22] were identical to three figures. The difference in the remaining five examples did not exceed 0.3%, that is, the corner point has an even smaller effect in the axisymmetric case than in the planar case.

The smallness of the dominant corner points, around which flow occurs with an attached shock wave, enabled us to seek close to optimum contours of planar nose shapes as a combination of rectilinear segments intersecting at a small angle $\Delta\vartheta_d$ at point $d$. A rapid method of constructing close to optimum generatrices with a single corner point was developed in [23] on the basis of these considerations. Here (see also, [11]), the optimum position of the corner point and the break angle at this point as well as the reduction in wave drag compared with wedges with the same $\tau$ are determined for all Mach numbers $1 \leq M_\infty \leq \infty$ and relative half-thicknesses of the nose shape $\tau = 1/l = y_f/x_f$. When $\Lambda_w < 0$, the optimum corner point is convex and located as shown in Fig. 5(a) [11, 23]. When $\Lambda_w > 0$, the flow past the optimum corner point is accompanied by the formation of a weak shock wave (Fig. 5b) which is located such that the reflected shock wave arrives at the point $f$, strictly speaking, analysis showed [11, 23] that, when $\Lambda_w > 0$, a close to optimum generatrix has two closely arranged dominant corner points of the same order: a first corner point past which there is a flow with the formation of centred wave and a second corner point past which there is a flow with the formation of a weak shock wave (Fig. 5c). When $\Lambda_w = 0$, the approach proposed in [11, 23] gives the exact result [12, 13], the optimum rectilinear generatrices.

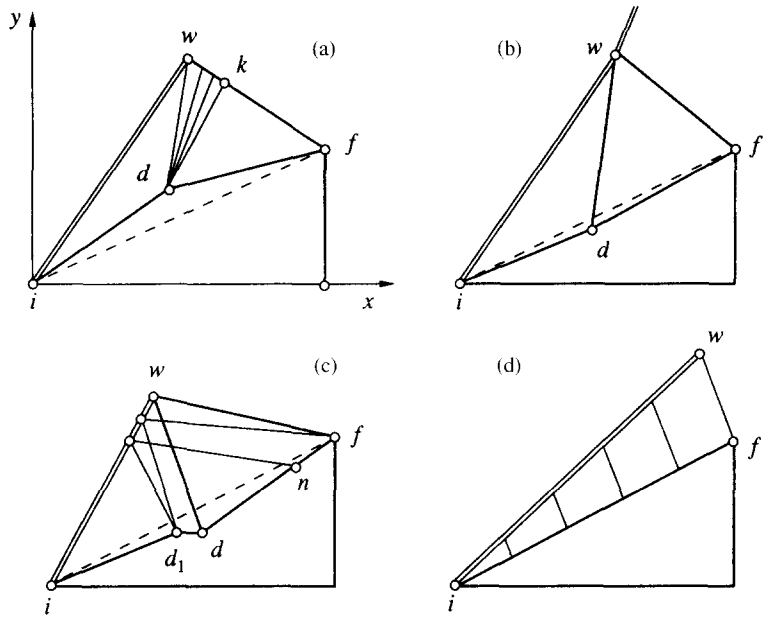


Fig. 5

However, this possibility is unique [11, 23]. A rectilinear generatrix is also optimum when $\Lambda_w \neq 0$ but the flow over it is sonic (Fig. 5d, the coincident $C^+$- and $C^-$-characteristics are normal to *if*).

Comparisons with the close to optimum planar contours with a single corner point from [20, 21] showed that their analogues from [11, 23] achieve no less than an 80–99% advantage compared with wedges. The almost instantaneous construction of thousands of close to optimum planar generatrices within the framework of the approach developed in [12, 23] enabled us to establish the value of the possible gains over the whole range of values of $M_\infty$ and $\tau$ corresponding to a supersonic flow with an attached shock wave. In the case of a perfect gas with $\kappa = 1.4$, the maximum gains in the wave drag coefficient are quantities of the order of 1.6% and these values are obtained in the case of hypersonic flow past fairly thick bodies ($\tau = 0.2 \ldots 0.5$). The gains in the domain corresponding to positive reflection coefficients do not exceed 1%. This makes the treatment of the contours with two corner points shown in Fig. 5c less urgent.

In the case shock waves of finite strength, for which $v_s, v > 0$, the ordinate of the shock way $y_\infty$ cannot vanish, by virtue of conditions (1.2) and (1.3) as, in this case, the first term in equality (1.2) would become infinite with a finite second term. Smooth generatrices of the type being considered cannot therefore originate in the axis of symmetry. On recalling the solution of the same problem in the approximation of Newton's equation, the first cause of the constraint obtained can be designated: the optimum nose shapes of bodies of revolution without a channel do not necessarily have to be pointed and to be in a flow with an attached shock wave. If this is so, the control contour method does not work since it is impossible to express the specified length of a body using an integral along a detached shock wave. If, however, the required optimum contour, in addition, contains a front face which, within the framework of Euler's equations, can turn out to be a section of a boundary extremum on account of the constraint on the length as previously, it is impossible moreover to formulate a condition of admissibility of just a unilateral variation in the abscissa of the front face using the method of an indefinite control contour. Finally, due to the unsmooth joints between the front face and the section of the two-sided extremum, the control contour method is again inapplicable for the same reason as in the case of the internal corner points discussed above.

The facts noted when developing the reasoning presented in [10, 24, 25] justify the consideration of nose shapes which are "suspected of being optimum" bodies with a front face $x = 0$ (when there is a constraint on the length), both in the approximation of Newton's formula and the Newton–Busemann formula, as nose shapes without a channel. Here, it is first necessary to determine the optimum size of the front face and to construct the optimum or close to optimum gently sloping generatrix which adjoins the front face with a corner point. These problems are solved in the next section taking the above into account. In the case of "short" nose parts, the smooth generatrices which are constructed satisfy all of the conditions for an extremum corresponding to their variation. If the maximum permissible length

is greater than a certain quantity, then the smooth, close to optimum, gently sloping sections which are constructed are analogous to the smooth contours from [11, 23]. Bodies of this type are called "long" bodies. Next, it has to be proved that the front face is a section of a boundary extremum. This problem is solved numerically by comparing the drags of bodies with a front face and the nose shapes obtained in the case of its permissible variations. The formulation and numerical solution of the so-called "conjugate" problem within the framework of the general method of Lagrange multipliers could become a similar alternative numerical check. In the case of nose shapes which are "suspected of being optimum" and Lagrange multipliers which satisfy the correctly formulated conjugate problem, the expression for the variation of the wave drag takes the form

$$\delta\chi = \ldots + X_d\Delta x_d + \int_0^{y_{d^\circ}} yX^\circ\delta x dy \tag{1.6}$$

The term, which is analogues to the right-hand side of equality (1.5) and only present in the case of "long" bodies, is denoted by the dots, the integral is taken along the front face *id* (Fig. 2a), $X_d$ and $X^\circ$ are functions of the flow parameters and the Lagrange multipliers, and $\Delta x_d$ and $\delta x$ are the increments in $x$ of the corner point and the variation of the abscissa of the front face. Non-negative values of $\Delta x_d$ and $\delta x$ are permissible. Hence, according to expression (1.6), the optimality conditions for the front face take the form $X_d \geq 0$ and $X^\circ \geq 0$. The formulation of the conjugate problem for short bodies, within the framework of the general method of Lagrange multipliers, is given in the appendix.

## 2. AXISYMMETRIC NOSE SHAPES WHICH ARE OPTIMUM OR CLOSE TO OPTIMUM WITH RESPECT TO WAVE DRAG

In this section "short" and "long" nose shapes are constructed which give, respectively, the minimum or close to minimum wave drag. Figures 2(a) and (b) explain the sense of the terms which have been introduced. In the case of a short nose shape (Fig. 2b), the characteristic *wcf* arriving at the terminal point *f* of the optimum contour *idf* intersects a part of the bunch of rarefaction waves from the $C+$-characteristic, which arises in the flow past the corner point at the junction of the front face *id* and the gently sloping section *df*. Coincidence of the points *w* and *c* corresponds to the boundary between short and long nose shapes. In the case of high aspect ratios, which correspond to long nose shapes, the $C^-$-characteristic *wf* is wholly located outside the above mentioned bunch of rarefaction waves (Fig. 2a).

According to the results presented below, the transition from short to long nose shapes, as a rule, occurs with aspect ratios $l$ which are close to unity and even less than unity. In this sense, the term "long" (nose shape) differs from the generally accepted meaning and, for a given $l$, it is not known before its generatrix has been constructed whether it will turn out to be short or long.

The construction of short and long nose shapes started out with a calculation of the flow past the axisymmetric front face. Euler's equations were integrated using the establishment process and the algorithms in [26–28] for calculating the domains of subsonic and transonic flow using a marching scheme and an algorithm for calculating supersonic flows with a variable orientation of the velocity vector. The basis of these algorithms is the Godunov scheme and its supersonic, steady-state analogue, their modifications [30–33] in the direction of increasing order of approximation in the subdomains of continuity of the parameters, and the method for constructing the bow shock wave described in [34]. An inclined, penetrable rectilinear boundary was specified behind the front face to which auxiliary (bordering) cells with constant parameters equal to the free-stream parameters are joined. Specification of this boundary ensures the accurate calculation of the bunch of rarefaction waves.

Examples of calculations carried out for certain values of the free-stream Mach numbers $M_\infty$ are shown in Fig. 6. Henceforth, the results presented correspond to the flow of a perfect gas with $\kappa = 1.4$ past the bodies. For each $M_\infty$, the bow shock wave, picked out during the course of the calculation over equal intervals $\Delta M = 0.1$ of the isomach line (the solid line is for $M = 1$) and several of the $C^+$-characteristics emerging from the corner point (the dashed lines) are shown. The latter characteristics were constructed using the parameter fields found by establishment by integration of the equation $dy/dx = \mathrm{tg}(\vartheta + \alpha)$. Figure 7 gives a representation of the difference meshes for a total number of cells of the order of $7 \times 10^5$. In this figure, twice as many thin mesh lines are shown along each direction for $M_\infty = 3$ which were used when calculating the flow past the front face (the left-hand part of Fig. 7) and a cone (the right-hand side) with a detached shock wave. The boundaries of the subdomains with meshes of a different structure were separated out and several of the streamlines, constructed by integration of the equation $dy/dx = \mathrm{tg}\vartheta$, have been sketched.

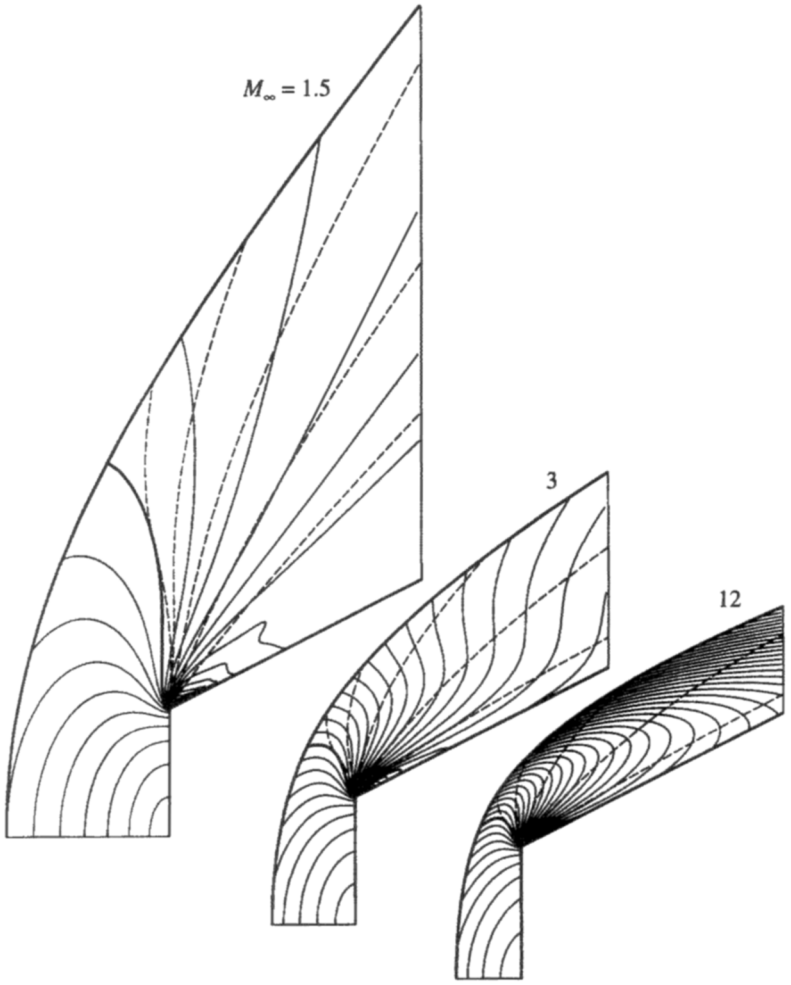


Fig. 6

The next stage in the construction procedure is the search for the required contour among the short optimum nose shapes for a specified aspect ratio $l = x_f/x_f$. Here, a family of closing, extremal $C^-$-characteristics $cf$ is constructed, the coordinates of the terminal point of which $f$ lie on the line $x = ly$, on account of which all of the nose shapes corresponding to them have the specified aspect ratio. The extremal $C^-$-characteristics $cf$ emerge from different points of the different closing $C^+$-characteristics of the bunch of rarefaction waves with its centre at the terminal point of the front face $d$. Use is made here of the condition for the total enthalpy $I$ to be constant in the whole of the flow

$$2i(p, \rho) + V^2 = 2I_\infty \equiv 2i(p_\infty, \rho_\infty) + V_\infty^2 \tag{2.1}$$

the dependence of the entropy $s$ on $\psi$ found when calculating the flow past the front face

$$s = S(\psi) \quad \text{when} \quad 0 \le \psi \le \psi_c \tag{2.2}$$

and, also, the necessary condition for an extremum (1.2) in $cf$ and the differential relations, including the compatibility condition in [10, 35] for a $C^-$-characteristic

$$\frac{dy}{d\psi} = \frac{\sin(\alpha - \vartheta)}{ky\rho V \sin\alpha}, \quad \frac{dx}{d\psi} = -\frac{\cos(\vartheta - \alpha)}{ky\rho V \sin\alpha}, \quad \frac{d\vartheta}{d\psi} - \frac{\operatorname{ctg}\alpha}{\rho V^2}\frac{dp}{d\psi} + \frac{\sin\vartheta}{ky^2\rho V} = 0 \tag{2.3}$$

Equations (2.3) were integrated with respect to $\psi$ from point $c$ of the chosen $C^+$-characteristic $dc$ of the bunch of rarefaction waves from $\psi = \psi_c > 0$ to $\psi_f = 0$ simultaneously with the solution of the finite

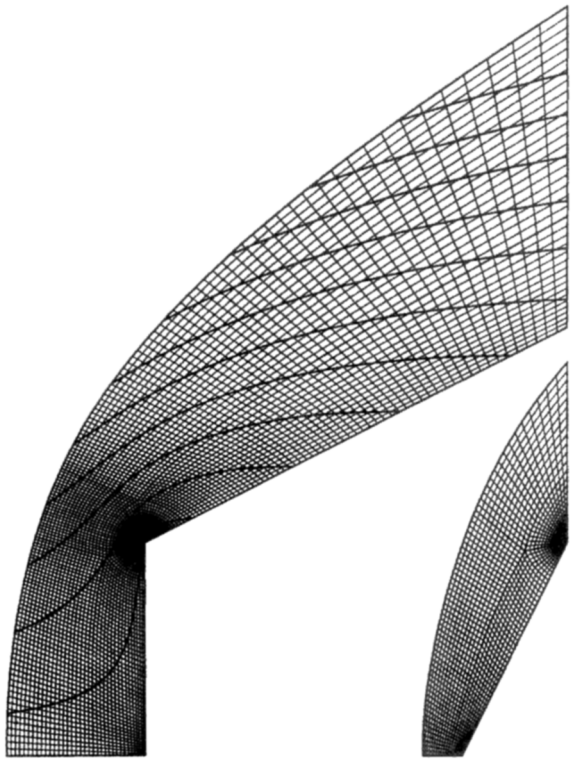

Fig. 7

equations (1.3), (2.1) and (2.2). The constant $\mu$ on the right-hand side of Eq. (1.3) was calculated using the parameters at the point $c$. In fact, Eq. (1.3) only served as a control. In the calculations, the result of the differentiation of Eq. (1.3) with respect to $\psi$, taking account of relations (2.1) and (2.2), the equation of state $i = i(p, \rho)$, the expressions for $a^2 = i_0/(1 - \rho i_p)$ and Eqs (2.3), was used instead of it. The resulting equation was integrated together with (2.3). If the aspect ratio $l$ is not high, the arbitrariness in the choice of the point $c$ in the closing $C^+$-characteristic of the bunch of rarefaction waves enabled us to find $x_f$ and $y_f$ such that their ratio is equal to $l$.

Execution of the procedure which has been described for different closing characteristics of the bunch gives a set of extremal $C^-$-characteristics $cf$ which, while corresponding to nose shapes with a specified $l$, have a different length and different wave drags $\chi$ in the scale of the fixed front fact. The wave drag is equal to the sum of the drag of the front face $id$ and the drag of the gently inclined section $\chi_{df}$. The drag $\chi_{df}$ was calculated as the difference between the corresponding flows along $cf$ and $dc$, and the wave drag coefficient $C_x$ takes account of the difference in the dimensions, where

$$C_x = \frac{\chi_{id} + \chi_{df}}{y_f^2} - p_\infty, \quad \chi_{df} = \int_f^c \left[ p \frac{\sin(\alpha - \vartheta)}{\rho V \sin\alpha} + u \right] d\psi - \int_d^c \left[ p \frac{\sin(\vartheta + \alpha)}{\rho V \sin\alpha} + u \right] d\psi$$

Henceforth, the normalizing factor in the expression for the stream function (see Eq. (2.3) and the formula for $y_\infty(\psi)$ after (1.3)) $k = 2$, and $V_\infty^\circ$, $\rho_\infty^\circ$ and $\rho_\infty^\circ (V_\infty^\circ)^2$ were taken as the velocity, density and pressure scales (the degree sign denotes dimensional quantities). Hence, $u_\infty = V_\infty = \rho_\infty = 1$ and $p_\infty = 1/(\kappa M_\infty^2)$.

Comparison of the coefficients $C_x$ for nose shapes constructed for different points $c$ either reveals the point which gives a minimum value of $C_x$ for a specified aspect ratio $l$ or it does not located such a point. The first possibility corresponds to the construction of a short nose shape which is suspected of a minimum wave drag (Fig. 8). The second possibility occurs when the point $c$, which ensures the specified aspect ratio, on rising to the shock wave along the $C^+$-characteristics, closing bunches of ever increasing strength is incident on it earlier than the minimum of $C_x$ is found. In these cases, the $C^-$-characteristic, arriving at the point $f$ of the required contour, starts out in the shock wave outside the initial bunch of rarefaction waves (Fig. 2a, $wf$ is the extremal closing $C^-$–characteristic).

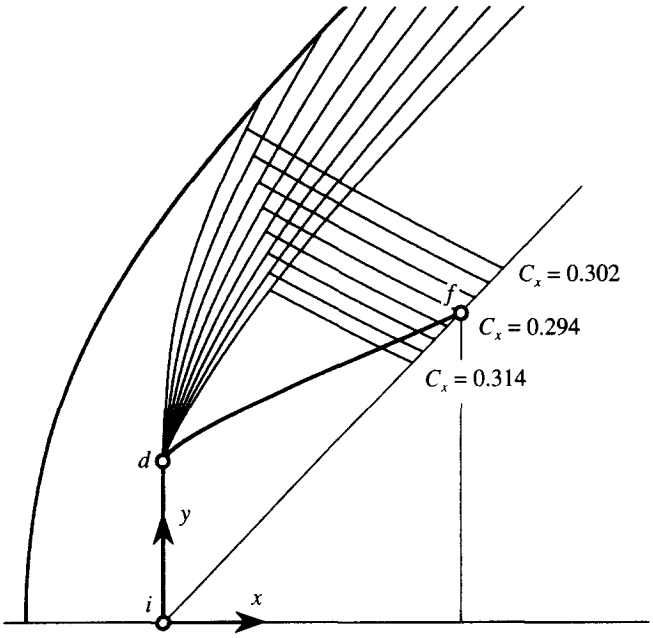


Fig. 8

The order of construction of the sections *df* close to optimum smooth (without corner points) long nose shapes differs from the order of construction of their short analogues. In the case of a chosen closing $C^+$-characteristic of a bunch with "centre" at the point *d*, the arbitrariness, which permitted the construction of short nose shape with a specified aspect ratio, consisted of the choice of the position of the point *c* on the above-mentioned characteristic. In the case of long nose shapes, the choice of the angle of inclination of the shock wave $\sigma_w$ at the point *w* plays the role of this arbitrariness (as well as in the selected closing $C^+$-characteristic $di°$) and $\alpha_\infty < \sigma_x < \sigma_{i°}$. For selected $\sigma_w$, the parameters behind it were initially determined using the relations in the shock wave. In the case of a perfect gas (the subscript *w* is omitted) [35]

$$p = p_\infty\left[1 + \frac{2\kappa}{\kappa+1}(M_\infty^2\sin^2\sigma - 1)\right], \quad \rho = \rho_\infty\left[\frac{\kappa-1}{\kappa+1} + \frac{2}{(\kappa+1)M_\infty^2\sin^2\sigma}\right]$$

$$u = V_\infty\left[1 - \frac{2}{\kappa+1}\left(\sin^2\sigma - \frac{1}{M_\infty^2}\right)\right], \quad v = V_\infty\frac{2}{\kappa+1}\left(\sin^2\sigma - \frac{1}{M_\infty^2}\right)\operatorname{ctg}\sigma \tag{2.4}$$

$$\operatorname{tg}\vartheta = \frac{v}{u}, \quad V = \sqrt{u^2+v^2}, \quad a = \sqrt{\frac{\kappa p}{\rho}}, \quad M = \frac{V}{a}$$

After the parameters behind the shock wave at the point *w* have been determined and arbitrary $x_w$ and $y_w > 0$ have been specified ($x_w = 0, y_w = 1$, for example), $\mu$ and $\mu°$ were calculated from equalities (1.2) and (1.3), written at this point. If the coefficient $\Lambda_w = 0$, then $\mu° = \mu$. Otherwise, $\mu° \neq \mu$ and, in the case of the "close to optimum" nose shape which is constructed later, the necessary condition for an extremum at the point *w*, mentioned in Section 1, is not satisfied. The simultaneous solution of Eqs (1.2), (2.1), (2.3) and (2.4) and the equation obtained by differentiating equality (1.3) with respect to $\psi$ enabled us to construct the sections $wi°$ and $wf°$ of the shock wave and the $C^-$-characteristic up to a point with a previously known $\sigma = \sigma_{i°}$. However, since the function $S(\psi)$ is now unknown in advance in the section $wf°$ of the extremal $C^-$-characteristic *wf*, the computational algorithm is different from that which has been described for constructing the extremal $C^+$-characteristic *cf* of a short nose shape.

The calculation of each pair of new points of the shock wave and the $C^-$characteristic, corresponding to a smaller value of $\psi$ and a larger value of $\sigma$, began with the specification of the value of $\sigma$. The necessary parameters behind the shock wave, to which the subscript *s* has been assigned, were then

found using formulae (2.4). The quantities $y_\infty$ and $\psi$ were determined using them and the parameters of the "preceding iteration" at the corresponding point of the extremal characteristic:

$$y_\infty = \frac{\mu^\circ V^2\sqrt{M^2-1}}{\rho_\infty u_\infty v_s(u_\infty - u_s)}\frac{p_s\rho}{p\rho_s}[(1+\Omega M^2)v + u\sqrt{M^2-1}]^{-1}, \quad \psi = y_\infty^2\rho_\infty u_\infty$$

All of the quantities without subscripts are parameters for the $C^-$-characteristic corresponding to the same $\psi$. In the first iteration, they are assumed to be equal to the parameters at its preceding point. The relation $S(\psi)$ was determined using the calculated $\psi$ and the parameters behind the shock wave, and a knowledge of this enabled us to find the parameters and coordinates of the new point of the $C^-$-characteristic using the method described earlier. The iterations were continued until convergence with respect to $\psi$ had been achieved and the calculation was continued until the value $\sigma = \sigma_{i^\circ}$ had been attained.

At the very beginning, $x_w$ and $y_w$ were specified arbitrarily. Hence, the coordinates of the terminal point of the bow shock wave obtained as a result were not identical to the known $x_{i^\circ}$ and $y_{i^\circ}$ from the calculation of the flow past the front face. Suppose $K$ is the ratio of $y_{i^\circ}$ to the value of the radial coordinate of the terminal point of the bow shock wave which has been found. The equations of the flow being considered are invariant under simultaneous multiplication of the $x$ and $y$ coordinates by any positive number and a shift along the axis of symmetry. In accordance with this, multiplication of the coordinates of the extremal shock wave which have been found and the $C^-$-characteristic by $K$, the multiplication of $\psi$ by $K^2$ and the necessary shift along the $x$ axis ensured matching of the coordinates and the stream function at the point.

When $0 = \psi_f \le \psi \le \psi_{i^\circ} = \psi_{f^\circ}$, the function $S(\psi)$ is known from the calculation of the flow past the front face. Hence, the section $f^\circ f$ of the characteristic $wf$ was constructed in the same way as the construction of the whole of the extremal characteristic in the case of short nose shapes. The arbitrariness in the choice of $\sigma_w$ enabled us to construct long, close to optimum nose shapes with a specified aspect ratio. By virtue of the integral law of conservation of the $x$ component of the momentum. the coefficient $C_x$ of the nose shapes constructed is equal to

$$C_x = \frac{1}{y_f^2}\int_{\psi_f=0}^{\psi_w}\left[p\frac{\sin(\alpha-\vartheta)}{\rho V\sin\alpha} + u\right]d\psi - \frac{\psi_w}{y_f^2}\left(\frac{1}{\kappa M_\infty^2}+1\right) - \frac{1}{\kappa M_\infty^2}$$

The close to optimum, long nose shapes was determined using the minimum of $C_x$ as a function of $y_{i^\circ}$. Figure 9 illustrates the construction of long, close to optimum nose shapes for $M_\infty = 3$. The increments $\Delta C_x = (C_x/C_x|_{\eta=1} - 1)\times 100$ as a function of $\eta = y_{i^\circ}/y_{i^+}$ are shown in this figure for different aspect ratios (the numbers on the curves). Here, $C_x|_{\eta=1}$ is the magnitude of the corresponding coefficient of a nose shape of fixed aspect ratio, constructed for $y_{i^\circ}/y_{i^+}$, $C_x$ is the value of them (for the same value of $l$) for nose shapes with $y_{i^\circ} > y_{i^+}$ and $i^+$ is a common point of the shock wave (Fig. 2a) and the $C^+$-characteristic $di^+$ which touches the sonic line. The values of $\mu$ at the points of minimum $C_x$ and $\Delta C_x$ are identical. The right-hand points of all of the curves correspond to the triangles $i^\circ wf^\circ$ which have degenerated to a point. The curve corresponding to $l = 1$ decreases monotonically without reaching a minimum. In the case of large $\mu$, there are no solutions with a triangle $i^\circ wf^\circ$ which ensure the equality $l = 1$. This means that the optimum nose shape for $l = 1$ is not long but short.

In the case of the curves constructed for $1.4 \le l \le 8.0$, there is a unique minimum, which is obtained at a fixed value of $y_{i^\circ}$. This corresponds to the solution in the class of short nose shapes (Fig. 2b) for which the initial point $c$ of the closing $C^-$-characteristic $cf$, when raised along the closing $C^+$-characteristic of the bunch of rarefaction waves with centre at the point $d$, turns out to be simultaneously also a point of the above-mentioned $C^+$-characteristic and the bow shock wave. Optimum (or close to optimum) nose shapes with large aspect ratios are obtained if the corresponding triangles $i^\circ wf^\circ$ (which are specific for each value of $l$) are constructed, in accordance with the scheme of Fig. 2(a), precisely at this point of the shock wave which arises in the flow past the front face. The constancy of $\mu$ at which the minima in the curves for $1.4 \le l \le 8.0$ are attained is also explained by this. Both for short as well as for long nose shapes, the optimum relative size of the front face $h = y_d/y_f$.

Up to now, it has been assumed that the front face is a section of a boundary extremum which appears on account of the constraint of the maximum permissible length of the nose section. We recall that, within the framework of Newton's formula, the front face is a section of a boundary extremum not only because of the constraint on the length but, also, by virtue of the restriction $0 \le \vartheta \le \pi/2$ on the applicability

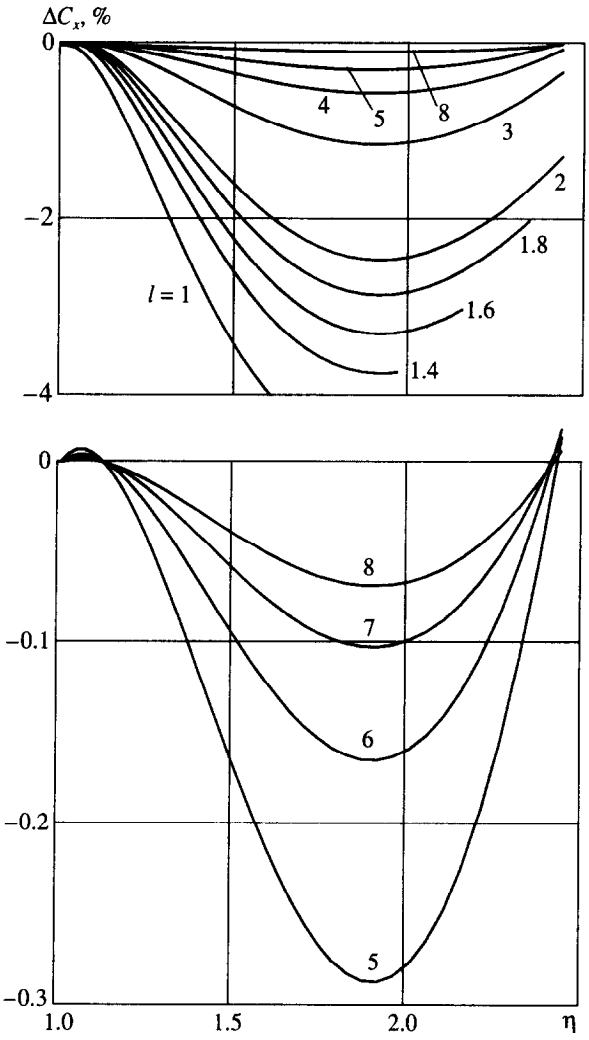


Fig. 9

of formula (1.1). In particular, this last restriction prohibits internal lunes (with $\delta x \geq 0$ when $0 \leq y < 1$), the introduction of which within the framework of Newton's formula reduces the drag by a quantity of the order of $(\delta x')^2$. The variations of a front face with $\Delta x_d \geq 0$, which are permissible within the framework of (1.1), with the optimum choice of its size and corner angle ($\vartheta_{d^+} = \pi/4$) lead to an increase in the drag (in the approximation of Newton's formula) which is proportional to $\Delta x_d$. Within the framework of Euler's equations, any variations of the front face which do not increase the length of the nose shape are permissible and the algorithms described above for constructing them still left open the question of the effect on $C_x$ of its permissible variation (which does not increase the length). The question of the optimality of a front face as a section of a boundary extremum has been investigated numerically.

The contours of a short nose shape, the contours obtained by three different methods of permissible variation of the front face and of the isomach line (with a step size $\Delta M = 0.05$, the solid curves are sonic lines), are shown in Fig. 10 for $M_\infty = 3$ and $l = 0.8$ and several of the $C^+$- and $C^-$-characteristics are sketched using dashed curves in Fig. 10(a). The values of $C_x$ presented in Fig. 10, found from the solution of the corresponding direct problems, confirmed that all the permissible variations of the front face increase the wave drag. The greatest increase was observed when the front face was "ground off" (Fig. 10b, $\Delta x_d = 0.05 y_d$), a noticeable increase was observed for a lune with an inclined tangent at the upper point (Fig. 10c, $\delta x_i = 0.1 y_d$, $\delta\vartheta_{d^-} \approx 17°$) and an insignificant increase was observed for a lune with a vertical tangent at the upper point (Fig. 10d, $\delta x_i = 0.1 y_d$, $\delta\vartheta_{d^-} = 0$).

The small increase in the drag coefficient in the last two cases and the fact that, in the approximation of Newton's formula, the front face is a bilateral extremum (which does not satisfy the required condition for a minimum $x' \geq 1$), made it advisable to use analogous (although also impermissible in the case of

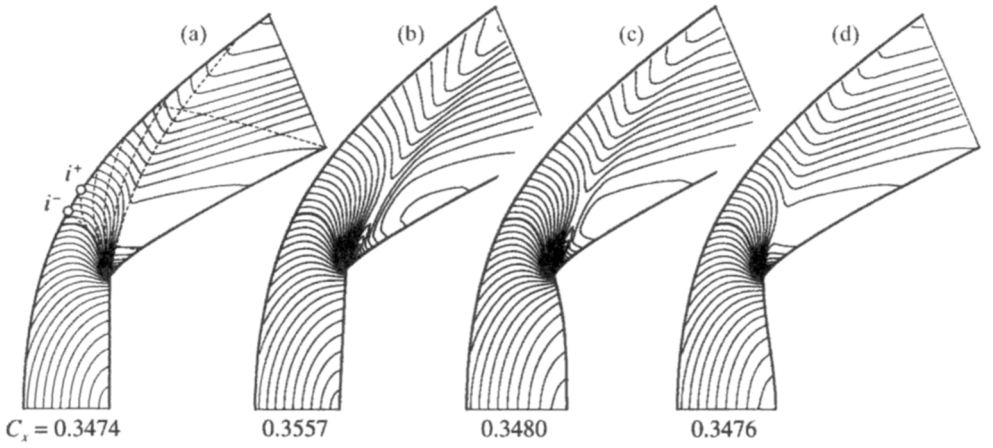


Fig. 10

a fixed aspect ratio) variations of the front face using a method which is symmetrical about the $y$ axis but with an increase in length. In the case of a variation with $\delta\vartheta_{d^-} = 0$, a decrease in the drag coefficient $C_x$ by the same magnitude as its decrease in the case of Fig. 10(d) was obtained, that is, the quantity $\delta C_x$ is proportional to $\delta x_i$ and the front face is not a section of a bilateral extremum.

The results of the calculation of short ($S$) and long ($L$) nose shapes are collected together in Table 1. The relative dimensions of their front faces $h = y_d/y_f$, the angles of inclination at the initial points $\vartheta_{d^+}$ and final points $\vartheta_f$ of their gently sloping sections $df$, the analogous characteristics of the optimum Newtonian bodies ($h^N$ and $\vartheta_f^N$ for $\vartheta_{d^+}^N = 45°$), the drag coefficients $C_x$ of the optimum or close to optimum nose shapes and the relative gains (as a percentage) of cones $\Delta C_x^{con}$, of Newtonian ($\Delta C_x^N$ is the first or unique number of the penultimate column) and optimum power-law bodies ($\Delta C_x^{m1}$ is the second number and $\Delta C_x^{m2}$ is the number in brackets) are presented together with $M_\infty$ and the aspect ratio $l$. If $C_x^{con}$, $C_x^N$ and $C_x^{mk}$ are the wave drag coefficients of the corresponding nose shapes calculated using Euler's equations, then $\Delta C_x^{con} = (C_x^{con}/C_x - 1) \times 100$ and $\Delta C_x^N$ and $\Delta C_x^{mk}$ are calculated in a similar manner. The values of $C_x^{m1}$ were taken from [36] where, for $M_\infty \geq 2$, the flow past blunt, single parameter optimum nose shapes of medium and large aspect ratio ($l \geq 1$) with a generatrix equation $y/y_f = (x/x_f)^m$ was calculated and the exponents $m$, which ensure that $C_x$ is a minimum for given values of $M_\infty$ and $l$, were determined. The values $C_x^{m2}$ of the optimum, pointed two parameter nose shapes were kindly provided by S.A. Takovitskii [37].

For a given aspect ratio $l > 0$, the construction of the optimum nose shape within the framework of Newton's formula begins (for example, see [11]) with the numerical determination of the root $x_f' \equiv q_f > 1$ of the transcendental equation

$$q_f(4q^2 + 3q^4 - 7 - 4\ln q)_f(1 + q_f^2)^{-2} = 4l \tag{2.5}$$

If $l > 4$, then $q_f \approx 4l/3$. After determining the root of Eq. (2.5), $h^N$ and $\vartheta_f^N$ were given by the formulae (the sign $\approx$ applies for $l > 4$)

$$h^N = \frac{4q_f}{(1+q_f^2)^2} \approx \frac{27}{2l(8l^2+9)}, \quad \vartheta_f^N = \operatorname{arctg}\frac{1}{q_f} \approx \operatorname{arctg}\frac{3}{4l} \approx \frac{3}{4l}$$

and the section $df$ of the Newtonian contour is constructed using the parametric relations

$$x = \frac{q_f}{4(1+q_f^2)^2}(4q^2 + 3q^4 - 7 - 4\ln q), \quad y = \frac{q_f(1+q^2)^2}{q(1+q^2)_f^2}, \quad 1 \leq x' \equiv q \leq q_f$$

If we change from $x$ and $y$ to $x^\circ = x/h^N$ and $y^\circ = y/h^N$, the equations take the universal form

$$x^\circ = (4q^2 + 3q^4 - 7 - 4\ln q)/16, \quad y^\circ = (1+q^2)^2/(4q), \quad 1 \leq x' \equiv q < \infty \tag{2.6}$$

Table 1

| $M_\infty$ | $l$ | $h\times10^3$ | $h^N\times10^3$ | $\vartheta_{d+}$, degree | $\vartheta_f$, degree | $\vartheta_f^N$, degree | $C_x\times10^4$ | $\Delta C_x^{con}$, % | $\Delta C_x^N$, $\Delta C_x^{m1}$ ($\Delta C_x^{m2}$), % | $\Delta C_{xNN}^{con}$, % |
|---|---|---|---|---|---|---|---|---|---|---|
| 1.5 (S) | 0.25 | 810 | 777 | 57 | 28 | 39 | 4316 | 50 | 6 | 21 |
| | 0.50 | 724 | 600 | 55 | 20 | 35 | 3469 | 75 | 24 | 32 |
| | 1.00 | 595 | 351 | 54 | 15 | 28 | 2548 | 102 | 43 | 33 |
| | 2.00 | 399 | 121 | 55 | 11 | 18 | 1578 | 101 | 33 | 25 |
| 1.5 (L) | 4.00 | 175 | 23 | 55 | 7 | 10 | 720 | 50 | 15 | 20 |
| | 8.00 | 42 | 3 | 55 | 3 | 5.3 | 241 | 48 | 12 (3.3) | 19 |
| | 12.0 | 15 | 1.0 | 55 | 1.8 | 3.6 | 117 | 57 | 16 (2.6) | 19 |
| | 20.0 | 4 | 0.2 | 55 | 0.9 | 2.1 | 45 | 77 | 25 (3.4) | 19 |
| 2 (L) | 2.00 | 297 | 121 | 55 | 14 | 18 | 1650 | 59 | 14, 12 | 25 |
| | 4.00 | 109 | 23 | 55 | 8 | 10 | 680 | 33 | 6.0, 3.8 | 20 |
| | 8.00 | 24 | 3 | 55 | 4 | 5.3 | 223 | 35 | 6.1, 2.4 (2.0) | 19 |
| | 12.0 | 10 | 1.0 | 55 | 2.2 | 3.6 | 109.4 | 44 | 9.7, 4.4 (2.1) | 19 |
| | 20.0 | 2.5 | 0.2 | 55 | 1.1 | 2.1 | 42.9 | 59 | 17, 9.0 (2.7) | 19 |
| 3 (S) | 0.25 | 784 | 777 | 61 | 34 | 39 | 5605 | 38 | 1.2 | 21 |
| | 0.50 | 654 | 600 | 59 | 29 | 35 | 4525 | 61 | 3.6 | 32 |
| | 1.00 | 452 | 351 | 58 | 24 | 28 | 3059 | 88 | 6.7 | 33 |
| 3 (L) | 2.00 | 238 | 121 | 57 | 17 | 18 | 1566 | 49 | 7.0 | 25 |
| | 4.00 | 79 | 23 | 57 | 10 | 10 | 605 | 28 | 2.9 (3.1) | 20 |
| | 8.00 | 18 | 3 | 57 | 5 | 5.3 | 198 | 27 | 2.7 (1.0) | 19 |
| | 12.0 | 6.5 | 1 | 57 | 2.8 | 3.6 | 98.9 | 32 | 4.7 (1.8) | 19 |
| | 20.0 | 2.3 | 0.2 | 57 | 1.4 | 2.1 | 39.9 | 43 | 9.4 (1.7) | 19 |
| 4 (S) | 0.25 | 776 | 777 | 61 | 35 | 39 | 5801 | 37 | 0.9 | 21 |
| | 0.50 | 633 | 600 | 60 | 31 | 35 | 4640 | 62 | 1.6 | 32 |
| | 1.00 | 430 | 351 | 56 | 27 | 28 | 3049 | 81 | 4.6, 21 | 33 |
| 4 (L) | 2.00 | 220 | 121 | 56 | 19 | 18 | 1499 | 49 | 5.5, 10 | 25 |
| | 4.00 | 71 | 23 | 56 | 11 | 10 | 558 | 28 | 2.4, 2.5 (2.4) | 20 |
| | 8.00 | 16 | 3 | 56 | 5 | 5.3 | 182 | 24 | 1.6, 1.0 (0.0) | 19 |
| | 12.0 | 6 | 1.0 | 56 | 3 | 3.6 | 91.4 | 27 | 2.8, 1.9 (0.9) | 19 |
| | 20.0 | 2 | 0.2 | 56 | 1.8 | 2.1 | 37.5 | 36 | 6.1, 3.5 (1.9) | 19 |
| 6 (S) | 0.25 | 770 | 777 | 62 | 36 | 39 | 5942 | 36 | 0.8 | 21 |
| | 0.50 | 615 | 600 | 60 | 33 | 35 | 4702 | 63 | 0.8 | 32 |
| | 1.00 | 420 | 351 | 54 | 28 | 28 | 3007 | 79 | 3.8, 20 | 33 |
| 6 (L) | 2.00 | 209 | 121 | 54 | 20 | 18 | 1428 | 51 | 4.7, 10 | 25 |
| | 4.00 | 65 | 23 | 54 | 12 | 10 | 506 | 31 | 2.4, 2.2 | 20 |
| | 8.00 | 15 | 3 | 54 | 6 | 5.3 | 161 | 23 | 0.9, 0.2 | 19 |
| | 12.0 | 7.8 | 1.0 | 54 | 4.0 | 3.6 | 81.4 | 23 | 1.1, 0.4 | 19 |
| | 20.0 | 2.2 | 0.2 | 54 | 2.2 | 2.1 | 33.9 | 28 | 3.0, 1.7 | 19 |
| 10 (S) | 0.25 | 765 | 777 | 62 | 37 | 39 | 6013 | 36 | 3.5 | 21 |
| | 0.50 | 608 | 600 | 60 | 34 | 35 | 4725 | 64 | 4.3 | 32 |
| | 1.00 | 419 | 351 | 52 | 29 | 28 | 2982 | 78 | 3.5, 20 | 33 |
| 10 (L) | 2.00 | 205 | 121 | 52 | 22 | 18 | 1382 | 53 | 4.3, 9.7 | 25 |
| | 4.00 | 63 | 23 | 52 | 13 | 10 | 466 | 36 | 2.3, 2.1 | 20 |
| | 8.00 | 14 | 3 | 52 | 7 | 5.3 | 140 | 27 | 1.2, 0.6 | 19 |
| | 12.0 | 5.5 | 1.0 | 52 | 4.9 | 3.6 | 69.9 | 23.0 | 0.9, 0.3 | 19 |
| | 20.0 | 2.4 | 0.2 | 52 | 2.8 | 2.1 | 29.3 | 22.6 | 1.3, 0.7 | 19 |

Within the framework of Euler's equations, the flow past precisely this body (one in the case of a fixed $M_\infty$) was calculated initially by establishment and then using the supersonic marching scheme. The $C_x^N$ of those of its initial sections which, in terms of $q_f$ from (2.5), correspond to the specified aspect ratio $l$, were simultaneously determined. For comparison, $C_x^{con}$ and $C_x^N$ were calculated using formula (1.1). On the cone $c_p = 1(1 + l^2)$ and on the front face $c_p = 1$. Taking this and relations (2.6) into account, we have

$$C_{xN}^{con} = \frac{1}{1+l^2},\quad C_{xN}^{N} = \frac{(3q^4+10q^2+4\ln q+2q^{-2}+17)_f}{32y_f^{\circ 2}} \approx \frac{27(8l^2+15)}{64l^2(4l^2+9)},\quad h^N = \frac{1}{y_f^\circ} \tag{2.7}$$

Table 2

| $M_\infty$ | $l$ | $K = M_\infty \tau$ | $\delta C_x^{con}$, % | $\delta C_x^N$, % | $\Delta C_{xNN}^{con}$, % | $\Delta C_{xNE}^{con}$, % |
|---|---|---|---|---|---|---|
| 1.5 | 0.25 | 6 | 45 | 71 | 21 | 42 |
| | 0.50 | 3 | 32 | 41 | 32 | 41 |
| | 1.00 | 1.5 | –3 | 3 | 33 | 41 |
| | 2.00 | 0.75 | –37 | –24 | 25 | 51 |
| | 4.00 | 0.375 | –45 | –41 | 20 | 31 |
| | 8.00 | 0.1875 | –57 | –52 | 19 | 33 |
| 3 | 0.25 | 12 | 22 | 37 | 21 | 36 |
| | 0.50 | 6 | 10 | 30 | 32 | 56 |
| | 1.00 | 3 | –13 | 15 | 33 | 76 |
| | 2.00 | 1.5 | –14 | –4 | 25 | 39 |
| | 4.00 | 0.75 | –24 | –21 | 20 | 24 |
| | 8.00 | 0.375 | –39 | –36 | 19 | 23 |
| 6 | 0.25 | 24 | 16 | 30 | 21 | 35 |
| | 0.50 | 12 | 4 | 28 | 32 | 62 |
| | 1.00 | 6 | –7 | 20 | 33 | 72 |
| | 2.00 | 3 | –7 | 7 | 25 | 44 |
| | 4.00 | 1.5 | –12 | –5 | 20 | 28 |
| | 8.00 | 0.75 | –22 | –20 | 19 | 22 |
| 12 | 0.25 | 48 | 15 | 28 | 21 | 35 |
| | 0.50 | 24 | 3 | 28 | 32 | 64 |
| | 1.00 | 12 | –6 | 22 | 33 | 72 |
| | 2.00 | 6 | –5 | 12 | 25 | 48 |
| | 4.00 | 3 | –7 | 5 | 20 | 34 |
| | 8.00 | 1.5 | –11 | –5 | 19 | 27 |

The subscript $N$ denotes that the corresponding coefficients were determined using Newton's formula. According to formula (2.7), $C_{xN}^{con}/C_{xN}^N \to 32/27 \approx 1.185$ when $l \to \infty$. The quantity $\Delta C_{xNN}^{con} = (C_{xN}^{con}/C_{xN}^N - 1) \times 100$ is shown in the last column of Table 1.

A comparison of $h$ and $h^N$ shows that the front faces of optimum Newtonian bodies are almost always smaller. The difference increases monotonically as the aspect ratio becomes larger and as $M_\infty$ decreases. The exceptions are the shortest bodies in the case of hypersonic velocities ($l = 0.25$, $M_\infty = 6$ and 10). Here, $h$ is somewhat less than $h^N$. The break angles at the corner point of Newtonian bodies are always larger ($\vartheta_{d+}^N = 45°$ and $\vartheta_{d+} = 52$–$62°$). An inverse inequality mainly holds for the angles of inclination at their terminal points. As a result, the gently inclined Newtonian sections are less convex. On account of this and the smaller angles of inclination to the $x$ axis, the pressure on the terminal sections of optimum bodies (close to the point $f$) is less than that on Newtonian bodies.

A comparison of the values of $\Delta C_x^N$, $\Delta C_x^{con}$ and $\Delta C_{xNN}^{con}$, that is, the losses of the cones, calculated within the framework of Newton's formula compared with the optimum Newtonian nose shapes exposes the advantages and disadvantages of Newton's formula. When $M_\infty \geq 3$, the quantity $\Delta C_x^N$ is 0.5–7% for all aspect ratios, that is, by one to two orders of magnitude less than $\Delta C_x^{con}$. For $M_\infty = 1.5$ and $0.5 \leq l \leq 8.0$, the magnitude of $\Delta C_x^N$ exceeds 10%, reaching a maximum of 43% for $l = 1$. However, $\Delta C_x^N$ is also 2.4–4 times less than $\Delta C_x^{con}$ in these cases. This is indicative of the surprising efficiency of Newton's formula in optimum profiling problems with an incorrect determination of the wave drag using it (see below). This property of Newton's formula has been revealed [11, 22, 38, 39] in problems of the optimum profiling of bodies in the flows with attached shock waves.

The excess $\Delta C_{xNN}^{con}$ of the drags of cones over the drags of Newtonian nose shapes within the framework of Newton's formula is much less in all of the examples for which calculations were carried out than in the approximation of Euler's equations. Table 2, where the drag coefficients $C_x$ of cones and Newtonian bodies, calculated using Newton's formula ($\Delta C_{xNN}^{con}$) and using Euler's equations ($\Delta C_{xNE}^{con}$), are compared, reveals the reason for this. The errors (as a percentage) of Newton's formula when calculating the values of $C_x$ for cones $\delta C_x^{con} = (C_{xN}^{con}/C_{xE}^{con} - 1) \times 100$ and Newtonian bodies ($\delta C_x^N$) are presented there. Newton's formula can both overestimate ($\delta C_x > 0$) and underestimate ($\delta C_x < 0$) the above-mentioned coefficients. However, it always "works in favour of" cones. Hence, within the framework of Newton's formula, cones lose out to Newtonian nose shapes to a far lesser extent than in the approximation of Euler's equations.

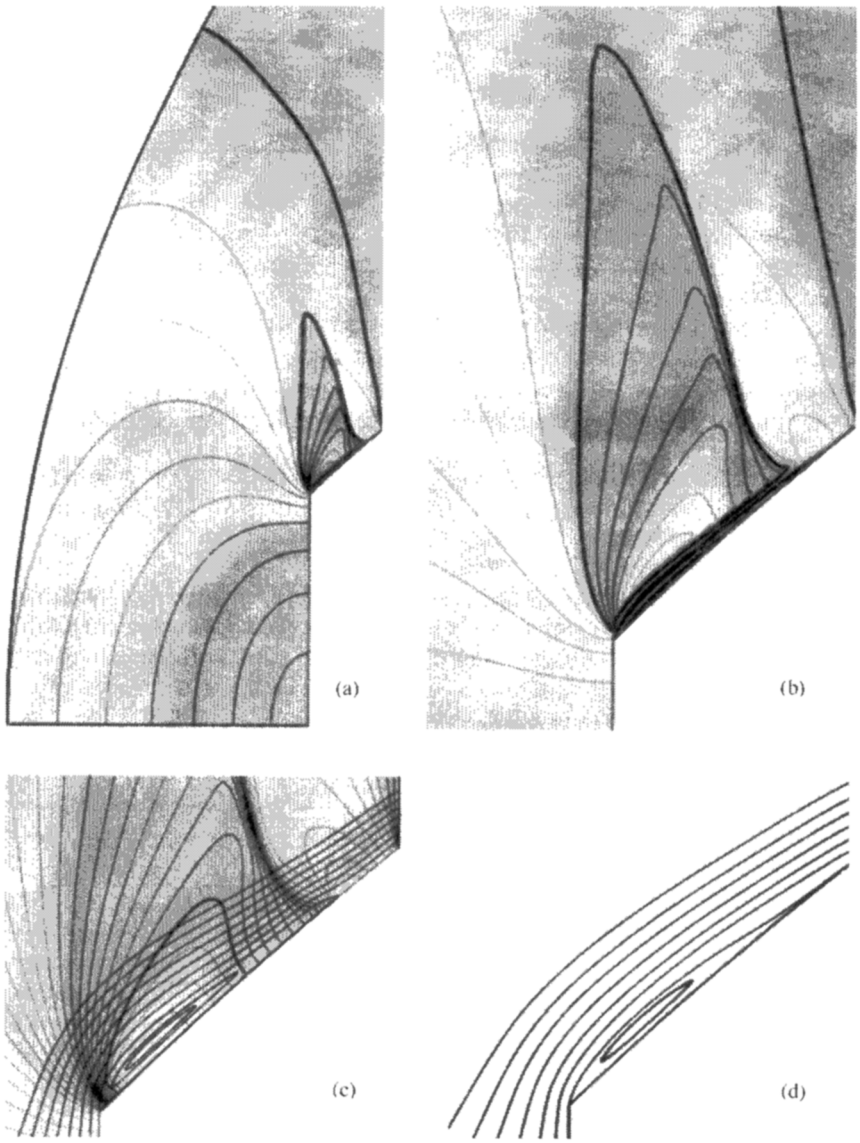


Fig. 11

Earlier, a comparison of their drag coefficients $C_x$ was only carried out using Newton's formula. Since $\Delta C_{x\mathrm{NN}}^{\mathrm{con}} < \Delta C_{x\mathrm{NE}}^{\mathrm{con}}$, it is very significant that such a comparison did not completely reveal the advantages of Newtonian nose shapes. In the case of cones when $M_\infty \geq 3$, an increase in the errors in Newton's formula as the hypersonic similarity parameter $K = M_\infty \tau$ is reduced [35] occurs when $l \geq 1$, when the shock wave is attached to the vertex of the cone.

Figure 11, which corresponds to $M_\infty = 1.5$ and $l = 0.25$, explains the reason for the increase in the drag coefficient $C_x$ of Newtonian bodies. The isomach lines (Fig. 11a and b, $\Delta M = 0.1$, the solid curves are the lines $M = 1$ and the blurred shock wave), isobars (Fig. 11b, $\Delta p/p_\infty = 0.05$, the solid curve is for $p/p_\infty = 1$) and the streamlines (Fig. 11c and d) are shown in this figure. In the flow past the corner point in this case, an overexpansion and subsequent stagnation of the flow occurs. On account of the stagnation, a closed supersonic zone with an acceleration of the gas up to $M > 1.6$ and $p/p_\infty < 0.8$ adjoins the corner point and with a detached, inviscid circulating flow close to the surface which is practically independent of the difference mesh (with an overall number of cells $N = 1656$, 6624 and 26496). The final acceleration of the flow up to supersonic velocity occurs on the main sonic line to the right of the closed supersonic zone. A calculation within the framework of the complete Reynolds equations and a differential model of turbulence [40–44] gave practically the same detached zone (Fig. 11d).

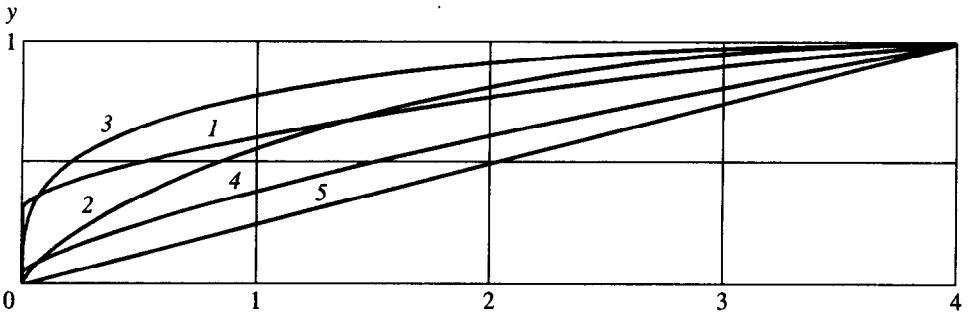


Fig. 12

In the case of Newtonian bodies with $l > y_*/x_*$, where $x_*$ and $y_*$ are the coordinates of the point of emergence from the contour of the $C^+$-characteristic touching the main sonic line, the flow in the vicinity of the front face remains the same as in Fig. 11. For $l = 0.25$, a domain of over expansion of the flow with a pressure of the order of and below $p_\infty$ occupies a considerable part of the gently inclined segment. The small increase in $C_x$ of the shortest Newtonian body (Table 1, $\Delta C_x^N = 6\%$) compared with the optimum nose shape is also explained by this. As $l$ increases, the domain of stagnation in the flat section with $p > p_\infty$ starts to make a large contribution. As a result, $\Delta C_x^N$ rapidly increases and attains a value of 43% when $l = 1$, then decreases when $l$ is increased further and, at large $l$, begins to become larger once again, reaching a value of 25% when $l = 20$. The behaviour of $\Delta C_x^N$ at other values of $M_\infty$ is similar but with values which become smaller as $M_\infty$ increases. For $M_\infty \geq 2$, a detached zone under a local supersonic zone did not arise.

The values of $\Delta C_x^{ml}$ for blunt, one-parameter optimum power-law nose shapes have been calculated [36] when $M_\infty = 2$ for $l \geq 2$ and, when $M_\infty \geq 4$, for $l \geq 1$. According to Table 1, in the case of the calculated values of $M_\infty$, $\Delta C_x^{ml} \approx 20\%$ when $l = 1$ and 10–12% when $l = 2$ for such bodies. When $l$ is increased further, the value of $\Delta C_x^{ml}$ decreases to a few percent and, for large values of $M_\infty$, to a few tenths of a percent and then increases again (up to 9% for $l = 20$ and $M_\infty = 2$). Pointed, two-parameter, optimum power-law nose shapes [37] can only be successfully constructed for sufficiently large values of $l$: when $M_\infty = 1.5$ and 2 for $l \geq 6$ and, when $M_\infty \geq 3$, for $l \geq 4$, that is, when the front face of the optimum nose shape is small. The values of $C_x^{m2}$ calculated in [37] for $M_\infty = 1.5$, 2, 3 and $10 \geq l \geq 6$ or 4 exceed the values of $C_x$ for an optimum nose shape by no more than 3.3%.

Concluding this section, we will now compare the nose shape which is optimum with respect to $C_x$ in this paper with the nose shapes in [45, 46] with the smooth contours

$$y = (x/l)^n(2 - x/l)^n, \quad 0 \leq x \leq l \tag{2.8}$$

with a constant exponent $n$, with respect to the values of $C_x$, the coefficients of frictional drag $C_f$ and total drag $C_D$. Depending on the flow conditions ($M_\infty$ and the Reynolds number Re, which is determined using the radius of the base and the free-stream parameters), $n$ was chosen in the range $0.3 \leq n \leq 0.7$. According to formula (2.8). Such nose shapes have a vertical tangent at the leading point (when $x = 0$) and a horizontal tangent at the end point (when $x = l$).

The comparison was carried out for $l = 4$, $M_\infty = 1.2$ and $Re = 7 \times 10^6$ when, according to the available results [45], the optimum exponent $n = 0.7$. For such $M_\infty$ and $l$, the optimum nose shape with a front face turned out to be short, that is, the nose shape which realizes the exact minimum in $C_x$. The contours of the optimum nose shape, of the two nose shapes described by formula (2.8) with $n = 0.7$ and 0.3, a Newtonian body and a cone are shown in Fig. 12 (curves 1, 2, 3, 4 and 5, respectively). While the volumes of the optimum nose shape and the nose shape described by formula (2.8) with $n = 0.7$ are practically equal, the volume of the nose shape described by formula (2.8) with $n = 0.3$ is 25% greater. The calculations were carried using well-known methods [40–44] within the framework of the complete Reynolds equations and the "$v_t$-90" differential model of turbulence. The results are given below

| Version | *1* | *2* | *3* | *4* | *5* |
|---|---|---|---|---|---|
| $C_x \times 10^4$ | 670 | 947 | 1033 | 962 | 1359 |
| $C_f \times 10^4$ | 83 | 84 | 95 | 75 | 53 |
| $C_D \times 10^4$ | 753 | 1031 | 1128 | 1038 | 1412 |
| $\Delta C_x$, % | 0 | 41 | 54 | 44 | 103 |
| $\Delta C_f$, % | 0 | 1 | 14 | –10 | –36 |
| $\Delta C_D$, % | 0 | 37 | 50 | 38 | 88 |

Here $\Delta C_x$ is the excess of the values of $C_x$ compared with the values of $C_x$ for the optimum nose shape (and similarly for $\Delta C_f$ and $\Delta C_D$) and the number of the version corresponds to the number on the generatrix in Fig. 12.

## 3. APPENDIX. FORMULATION OF THE PROBLEM OF CONSTRUCTING SHORT OPTIMUM NOSE SHAPES BY THE GENERAL METHOD OF LAGRANGE MULTIPLIERS

The problem of the profiling of short nose shapes which, for a specified aspect ratio, achieve a minimum value of the coefficient $C_x$ has been solved in Section 2. It was established numerically there that, for permissible variations of the front face, the coefficient $C_x$ of the constructed nose shape increases. We will now show to what the proof of this fact within the framework of the method of Lagrange multipliers reduces [10].

The flow domains, in which the conjugate problem for Lagrange multipliers is formulated and solved, are shown in Fig. 2(b). The flow in the domain $\Omega$ with a boundary $\partial\Omega$, consisting of the shock wave $i_0w$, the section of the axis of symmetry $i_0i$, the front face $id_-$, the flat section $d_+f$ and the $C^-$-characteristic $fw$, is described by the equations

$$\begin{aligned} &L_k \equiv \frac{\partial a^{(k)}}{\partial x} - \frac{\partial b^{(k)}}{\partial y} = 0, \quad k = 1, 2, 3 \\ &a^{(1)} = y\rho u, \quad b^{(1)} = -y\rho v, \quad a^{(2)} = yp + y\rho u^2, \quad b^{(2)} = -y\rho uv \\ &a^{(3)} = y\rho us, \quad b^{(3)} = -y\rho vs \end{aligned} \tag{3.1}$$

with the impermeability

$$L \equiv a^{(1)} + x' b^{(1)} = 0 \tag{3.2}$$

in the front face $id_-$ and in the section $d_+f$, the condition $\vartheta = 0$ in the section $i_0i$ of the $x$ axis and with relations in the section $i_0w$ of the nose shape. In Fig. 2(b), the points $d_-$, $d_+$ and $d$ coincide. However, the flow parameters at these points are different. We will write the shock-wave equation in the form

$$L^w \equiv x' - \Sigma = 0 \tag{3.3}$$

In the case of a fixed free stream, the quantity $\Sigma = \mathrm{ctg}\sigma$ defines all the flow parameters behind the shock wave. Using this quantity, two of the four conservation laws in the bow shock wave can be written in the form (parameters behind the shock wave have no subscripts)

$$a^{(1)} + \Sigma b^{(1)} = a_\infty^{(1)} + \Sigma b_\infty^{(1)}, \quad a^{(2)} + \Sigma b^{(2)} = a_\infty^{(2)} + \Sigma b_\infty^{(2)} \tag{3.4}$$

Apart from a term and a multiplier which are unimportant in the solution of the variational problem, the nose section wave drag is equal to

$$\chi = \left( \int_i^{d_-} + \int_{d_+}^{f} \right) yp\,dy \tag{3.5}$$

The distribution of $p$ on $idf$ and, consequently, also $\chi$ are determined by the solution of Eqs (3.1) for the conditions formulated above, including (3.2)–(3.4) in $idf$, the section $i_0i$ of the $x$ axis and in the shock wave $i_0w$. In accordance with this and acting within the framework of the method of Lagrange multipliers, we formulate the functional

$$I = \chi + \left( \int_i^{d_-} + \int_{d_+}^{f} \right) \nu L\,dy + \int_{i_0}^{w} \lambda L^w dy + \iint_\Omega \mu_k L_k\,dx\,dy \tag{3.6}$$

in order to obtain the required optimality conditions.

Henceforth, $\nu = \nu(y)$, $\lambda = \lambda(y)$ and $\mu_k = \mu_k(x, y)$, which are to be determined from the solution of the conjugate problem which is formulated later, are undetermined Lagrange multipliers and summation is assumed over repeated indices $k = 1, 2$ and 3.

By virtue of the definitions of $L$, $L^w$ and $L_k$ from equalities (3.1)–(3.3), the variations of the functional $I$, introduced by equality (3.6) and the variations of the optimizing functional $\chi$, defined by formula (3.5), are identical for any permissible variations of the contour *idf*, that is $\delta\chi = \delta I$. Hence, by acting in accordance with the rules which take account of the form of expression (3.5), the fact that inequalities (3.4) are satisfied in the bow shock wave, the singularities in the calculation of the contribution to $\delta I$ due to variation of the coordinates of the corner point $d$ and the possibility of discontinuities in the Lagrange multipliers $\mu_k(x, y)$ in the case of continuous flow parameters and other factors described in [10], we arrive at an expression for the variation $\delta\chi = \delta I$. Together with variations of the controls (the functions $x = x(y) = 0$, when $0 \le y \le y_d$, and $x = x(y)$, when $y_d \le y \le y_f$, and the coordinates $x_d$ and $y_d$ of the corner point) in the expression for $\delta\chi$, variations of the flow parameters ("of the phase variables"), that is, of the $u$ and $\upsilon$ components of the velocity vector and the entropy $s$ and, also, of the abscissa $x = x(y)$ and the inclination of the shock wave $\sigma = \sigma(y)$ or the quantity $\Sigma = \mathrm{ctg}\sigma$ occur, which are due to variations in the shape of the nose section. Dealing with the arbitrarinesses in the choice of the undetermined Lagrange multiplier, introduced when constructing the functional (3.6), we change the multipliers in front of the variations of the phase variables for any (not necessarily optimum) nose shape contour to zero. As a result, we obtain the so-called conjugate problem for Lagrange multipliers and only the variations of the controls remain in the expression for $\delta\chi$, which enables one to formulate the necessary conditions for $\chi$ to be a minimum.

In formulating the conjugate problem, we initially write the terms of the expression for $\delta\chi$ with variations of some of the phase variables (denoting the remaining variations by dots) and, then, the equations and conditions which follow when the coefficients accompanying them are equated to zero. We begin with $\delta u$, $\delta\upsilon$ and $\delta s$ in $\Omega$. By what has been said above, we have

$$\delta\chi = \ldots + \iint_{\Omega} (R^u \delta u + R^\upsilon \delta\upsilon + R^s \delta s)\,dx\,dy$$

where

$$\begin{aligned}
R^u &\equiv a_u^{(1)}\frac{\partial\mu_1}{\partial x} - b_u^{(1)}\frac{\partial\mu_1}{\partial y} + a_u^{(2)}\frac{\partial\mu_2}{\partial x} - b_u^{(2)}\frac{\partial\mu_2}{\partial y} + a_u^{(3)}\frac{\partial\mu_3}{\partial x} - b_u^{(3)}\frac{\partial\mu_3}{\partial y} = 0\\
R^\upsilon &\equiv a_\upsilon^{(1)}\frac{\partial\mu_1}{\partial x} - b_\upsilon^{(1)}\frac{\partial\mu_1}{\partial y} + a_\upsilon^{(2)}\frac{\partial\mu_2}{\partial x} - b_\upsilon^{(2)}\frac{\partial\mu_2}{\partial y} + a_\upsilon^{(3)}\frac{\partial\mu_3}{\partial x} - b_\upsilon^{(3)}\frac{\partial\mu_3}{\partial y} = 0\\
R^s &\equiv a_s^{(1)}\frac{\partial\mu_1}{\partial x} - b_s^{(1)}\frac{\partial\mu_1}{\partial y} + a_s^{(2)}\frac{\partial\mu_2}{\partial x} - b_s^{(2)}\frac{\partial\mu_2}{\partial y} + a_s^{(3)}\frac{\partial\mu_3}{\partial x} - b_s^{(3)}\frac{\partial\mu_3}{\partial y} = 0\\
a_u^{(k)} &= \frac{\partial a^{(k)}}{\partial u}, \quad a_\upsilon^{(k)} = \frac{\partial a^{(k)}}{\partial\upsilon}, \quad a_s^{(k)} = \frac{\partial a^{(k)}}{\partial s}, \ldots
\end{aligned} \tag{3.7}$$

The well-known thermodynamic equalities

$$Tds = di^\circ - \omega^\circ dp, \quad \omega^\circ = i_p^\circ, \quad a^{-2} = \rho_p^\circ = -\rho^2\omega_p^\circ = -\rho^2 i_{pp}^\circ \tag{3.8}$$

and the condition for the total enthalpy (2.1) to be constant were taken into account when calculating the derivatives of $a^{(k)}$ and $b^{(k)}$. In equalities (3.8) $\omega^\circ = 1/\rho^\circ$ is the specific volume, a degree sign superscript is assigned to thermodynamic parameters, that is, to known functions of $p$ and $s$, and partial derivatives with respect to $p$ for constant $s$ are denoted by the subscript $p$. On calculating the coefficients of system (3.7), taking account of relations (3.8), we reduce it to the form

$$\begin{aligned}
&u\frac{d\mu_1}{dt} - a^2\frac{\partial\mu_1}{\partial x} + (u^2 - a^2)\frac{d\mu_2}{dt} + su\frac{d\mu_3}{dt} - sa^2\frac{\partial\mu_3}{\partial x} = 0, \quad \frac{d}{dt} \equiv u\frac{\partial}{\partial x} + \upsilon\frac{\partial}{\partial y}\\
&\frac{d\mu_1}{dt} + u\frac{d\mu_2}{dt} + \frac{p}{\rho}\frac{\partial\mu_2}{\partial x} + (s-1)\frac{d\mu_3}{dt} = 0\\
&(a^2 - \upsilon^2)\frac{d\mu_1}{dt} - a^2 u\frac{\partial\mu_1}{\partial x} + u(a^2 - \upsilon^2)\frac{d\mu_2}{dt} - a^2 V^2\frac{\partial\mu_2}{\partial x} + s(a^2 - \upsilon^2)\frac{d\mu_3}{dt} - sa^2 u\frac{\partial\mu_3}{\partial x} = 0
\end{aligned} \tag{3.9}$$

System (3.9) has the same characteristics as the flow equations (3.1). At any velocities, these are streamlines ($C^0$-characteristics), along which

$$\left(M^2 - 1 + \frac{V^2\rho_s^\circ}{\rho T}\right)\left(\frac{d\mu_1}{dt} + u\frac{d\mu_2}{dt} + s\frac{d\mu_3}{dt}\right) - u\frac{d\mu_2}{dt} + \frac{V^2}{T}\frac{d\mu_3}{dt} = 0 \tag{3.10}$$

with the operator $d/dt$ defined by the second relation of (3.9) and with $\rho_s^\circ = (\partial\rho^\circ/\partial s)_p$. If the density is given, not as a function of $p$ and $s$ but of $p$ and $i$, that is, $\rho = \rho(p, i)$, then, by virtue of equalities (3.8),

$$\rho_s^\circ = -\rho T\rho_p < 0 \tag{3.11}$$

The equations of system (3.9), which are independent of Eq. (3.10), can be written in the form

$$(a^2 - u^2)\left(\frac{\partial\mu_1}{\partial x} + s\frac{\partial\mu_3}{\partial x} + \frac{d\mu_2}{dt}\right) - uv\left(\frac{\partial\mu_1}{\partial y} + s\frac{\partial\mu_3}{\partial y}\right) = 0$$

$$(a^2 - V^2)\left(\frac{\partial\mu_1}{\partial x} + s\frac{\partial\mu_3}{\partial x}\right) + (u^2 - a^2)\left(v\frac{\partial\mu_2}{\partial y} - u\frac{\partial\mu_2}{\partial y}\right) = 0$$

When $V > a$, the $C^-$-characteristics are characteristics of this system. Along these characteristics, $\mu_1$, $\mu_2$ and $\mu_3$ satisfy the differential relations

$$d\mu_1 + V\frac{\cos(\vartheta \pm \alpha)}{\cos\alpha}d\mu_2 + sd\mu_3 = 0 \tag{3.12}$$

with the upper (lower) sign for the $C^+(C^-)$-characteristics.

On the generatrix of the body $idf$, the variations in $s$, corresponding to a streamline which has passed across the direct shock wave, are equal to zero. Hence, here, with a different meaning of the variations from that above (in the integral over $\Omega$, the variations are differences in the values for fixed $x$ and $y$ and, now, in the shock wave, they are differences in the values for a fixed $y$ and for the abscissae of the corresponding points which have been displaced together with the generatrix or the shock wave [10]), we obtain

$$\delta\chi = \ldots + \left(\int_i^{d_-} + \int_{d_+}^{f}\right)(B^u\delta^\circ u + B^v\delta^\circ v)dy = 0$$

where

$$B^u \equiv -a^{(1)} + \mu_k(a_u^{(k)} + b_u^{(k)}\operatorname{ctg}\vartheta) + \nu(a_u^{(1)} + b_u^{(1)}\operatorname{ctg}\vartheta) = 0$$

$$B^v \equiv b^{(1)} + \mu_k(a_v^{(k)} + b_v^{(k)}\operatorname{ctg}\vartheta) + \nu(a_v^{(1)} + b_v^{(1)}\operatorname{ctg}\vartheta) = 0$$

The equation for determining the multiplier $\nu(y)$ and the boundary condition relating $\mu_k$ in the generatrix of the nose shape follow from this. Since $\operatorname{ctg}\vartheta = 0$ in the front face, we shall write them separately for the front face and the flat segment

$$\nu = -\mu_1 - s\mu_3, \quad \mu_2 = -1 \quad \text{in} \quad id_-, \quad \nu = u - \mu_1 - s\mu_3, \quad \mu_2 = -1 \quad \text{in} \quad d_+f \tag{3.13}$$

In the closing $C$-characteristic $fw$, the variations have the same meaning as in the domain $\Omega$ when there is no variation in $x$. As a result, we shall have

$$\delta\chi = \ldots + \int_f^w (C^u\delta u + C^v\delta v + C^s\delta s)dy$$

where

$$C^r \equiv \mu_k\{a_r^{(k)} + b_r^{(k)}\operatorname{ctg}(\vartheta - \alpha)\} = 0, \quad r = u, v, s \tag{3.14}$$

Since $fw$ is a $C^-$-characteristic, of the three equations (3.14) only two relating the multipliers $\mu_k$ in $fw$ are independent. They have the form

$$\mu_1 + \xi_+\mu_2 + s\mu_3 = 0, \quad \mu_3 + \eta_-\mu_2 = 0 \tag{3.15}$$

where the notation

$$\xi_{\pm} = V\frac{\cos(\vartheta \pm \alpha)}{\cos\alpha}, \quad \eta_{\pm} = \frac{\rho_s^{\circ} V}{\rho}\sin\vartheta\,\mathrm{tg}\alpha + \frac{T\sin(\vartheta \pm \alpha)}{V\sin\alpha}$$

has been used (with the derivative $\rho_s^{\circ}$, which is conveniently found using formula (3.11).

According to the last condition of (3.13), $\mu_{2f} = -1$. $\mu_{1f}$ and $\mu_{3f}$ are found from this and from Eqs (3.15), and $\mu_1$, $\mu_2$ and $\mu_3$ in *fw* are then determined from the simultaneous solution of the finite equations (3.15) and the differential equation (3.12) with the minus sign.

In the section $i_0 i$ of the axis of symmetry, the variations $\delta\upsilon = \delta s = 0$. Hence,

$$\delta\chi = \ldots + \int_{i_0}^{i} A^u \delta u dx$$

where

$$A^u \equiv \mu_k b_u^{(k)} = 0 \tag{3.16}$$

The $b_u^{(k)}$ occurring here are of the order of $y\upsilon$. Hence, if, on approaching the $x$ axis, the multipliers $\mu_k$ are bounded or increase more slowly than $1/(y\upsilon)$, the condition (3.16) is automatically satisfied. The constraint on $\mu_k$, which follows from it, can be written in the form

$$\lim_{y\to 0}(\mu_k y\upsilon) = 0, \quad k = 1, 2, 3 \tag{3.17}$$

Behind the bow shock wave, the variations in all of the parameters are expressed in terms of $\delta^{\circ}\Sigma$. Moreover, the variation in the shock wave abscissa is $\delta^{\circ}x$. Finally, the contribution of the section $i_0 w$ of the shock wave to the variation $\delta\chi$ and the equation and conditions which follow from it take the form

$$\delta\chi = \ldots - \lambda_{i_0}\Delta x_{i_0} + \lambda_w\{\mathrm{ctg}(\vartheta - \alpha) - \Sigma\}_w \Delta y_w + \int_{w}^{i_0}(W^{\Sigma}\delta^{\circ}\Sigma + W^x\delta^{\circ}x)dx$$

$$W^{\Sigma} \equiv \lambda - (\mu_1 + s\mu_3)b^{(1)} - \mu_2 b^{(2)} + \mu_3 a_{\infty}^{(1)}\varphi_{\Sigma} = 0 \quad \left(\varphi_{\Sigma} = \upsilon\frac{u - u_{\infty}}{T}\right) \tag{3.18}$$

$$W^x \equiv \frac{d\lambda}{dy} - \mu_k\frac{db^{(k)}}{dy} = 0, \quad \lambda_w = 0 \tag{3.19}$$

Here, $\varphi_{\Sigma} = ds/d\Sigma$, $d/dy$ is a derivative with respect to $y$ along the shock wave, the multiplier $\lambda(y)$ is a continuous function of $y$ and the expression for $\varphi_{\Sigma}$ is taken from [10, p. 435].

Condition (3.18) is satisfied in the whole of the shock wave section $i_0 w$, including at the point $i_0$. Since, $a_{\infty}^{(1)}\varphi_{\Sigma} \sim y\upsilon$ at this point, $\lambda_{i_0} = 0$ according to conditions (3.17) and (3.18). Finally, all the terms on the right-hand side of the last expression for $\delta\chi$ disappear.

The relation between the Lagrange multipliers at this point is obtained from the last condition of (3.19) and condition (3.18) written at the point $w$.

$$(\mu_1 + s\mu_3)_w b_w^{(1)} - \mu_{2w} b_w^{(2)} + \mu_{3w} a_{\infty}^{(1)}\varphi_{\Sigma w} = 0 \tag{3.20}$$

On the other hand, as has been explained earlier, the values of $\mu_{kw}$ at the above-mentioned point have already been determined and, in the general case, they do not satisfy condition (3.20). Consequently, the $C^+$-characteristic *dw*, which arrives at the point $w$, will be a line of discontinuity of the multipliers $\mu_k$. This will only not be so if their limiting values, found from relations which are satisfied on the $C^-$-characteristic *wf*, satisfy condition (3.20). It can be shown that this condition is satisfied if the reflection coefficient $\Lambda_w$ is equal to zero at the point $w$ or, what is the same thing, condition (1.4) is satisfied. In this connection, we shall assume that lines of discontinuity of $\mu_k$ exist in the case of continuous flow parameters. Their contribution to the variation $\delta\chi$ and the conditions in such discontinuities which follow from it take the form

$$\delta\chi = \ldots + \int (D^u \delta u + D^v \delta v + D^s \delta s) dy$$
$$D^r \equiv [\mu_k](a_r^{(k)} + x' b_r^{(k)}) = 0, \quad k = u, v, s \tag{3.21}$$

The integral is taken along all lines of discontinuity belonging to the domain $\Omega$; $x' = dx/dy$ along such lines and $[\mu_k]$ is the difference between the values of $\mu_k$ at a discontinuity.

The system of homogeneous equations (3.21) in $[\mu_k]$ only has non-zero solutions in the case of $x'$ determining the $C^0$- and $C^{\pm}$-characteristics. At the same time, only two conditions, which are imposed on the discontinuities $\mu_k$, are obtained from the three equalities (3.21). On the $C^0$-characteristics, we have

$$x' = \operatorname{ctg}\vartheta, \quad [\mu_2] = 0, \quad [\mu_1] + s[\mu_3] = 0 \tag{3.22}$$

while, on the discontinuities of the $C^+$- and $C^-$-characteristics

$$x' = \operatorname{ctg}(\vartheta \pm \alpha), \quad [\mu_1] + \xi_{\mp}[\mu_2] + s[\mu_3] = 0, \quad [\mu_3] \mp \eta_{\pm}[\mu_2] = 0 \tag{3.23}$$

The upper(lower) signs correspond to the $C^+(C^-)$-characteristics.

Differential equation (3.1) is satisfied from both sides of the discontinuous $C^0$-characteristic. If the streamline is not a tangential discontinuity, that is, the parameters on it continuous, then, taking account of the constancy of $s$ along a streamline, we find

$$\left(M^2 - 1 + \frac{V^2 \rho_s^\circ}{\rho T}\right)\left(\frac{d[\mu_1 + s\mu_3]}{dt} + u\frac{d[\mu_2]}{dt}\right) - u\frac{d[\mu_2]}{dt} + \frac{V^2}{T}\frac{d[\mu_3]}{dt} = 0$$

Together with condition (3.22), this gives that, along a continuous $C^0$-characteristic

$$[\mu_2] = 0, \quad [\mu_1] = \text{const}, \quad [\mu_3] = \text{const} \quad \text{in} \quad C^0 \tag{3.24}$$

Using the same method, we obtain from Eqs (3.12)

$$d[\mu_1] + \xi_{\pm} d[\mu_2] + s d[\mu_3] = 0$$

Hence, from relations (3.23), the equality

$$d\rho = \rho_s^\circ ds + \rho_p^\circ dp = \rho_s^\circ ds - \rho V a^{-2} dV$$

and the compatibility conditions which are satisfied on the $C^{\pm}$-characteristics, we find

$$[\mu_2]^2 y \rho V^2 \sin^2\vartheta \operatorname{tg}\alpha = \text{const}, \quad [\mu_1] = -\xi_{\mp}[\mu_2] - s[\mu_3], \quad [\mu_3] = \pm\eta_{\pm}[\mu_2] \tag{3.25}$$

where, as everywhere, the upper (lower) signs correspond to $C^+(C^-)$-characteristics.

Conditions (3.15) on the $C^-$-characteristic *fw* differ from conditions (3.23) at the discontinuities of the $C^-$-characteristics only in the notation which is used ($\mu_k$ instead of $[\mu_k]$). On *fw*, the multipliers $\mu_k$ are therefore determined by the finite relations

$$\mu_2^2 y \rho V^2 \sin^2\vartheta \operatorname{tg}\alpha = \text{const}, \quad \mu_1 = -\xi_+\mu_2 - s\mu_3, \quad \mu_3 = -\eta_-\mu_2 \tag{3.26}$$

and by the corollary of condition (3.13), which is satisfied on $d_+f$, $\mu_{2f} = -1$. These relations will be required later and, for the present, we will turn to the discontinuities in the multipliers $\mu_k$.

We shall assume that, on the closed $C^-$-characteristic *fw*, the discontinuity $\mu_k$ arrived along the characteristic of another family ($C^0$ or $C^+$). Then, in addition to equalities (3.22) or (3.23), the two additional conditions

$$[\mu_1] + \xi_+[\mu_2] + s[\mu_3] = 0, \quad [\mu_3] + \eta_-[\mu_2] = 0$$

are satisfied at the point of intersection by virtue of conditions (3.15), which are satisfied on *fw*. It follows from this and from the corresponding equalities (3.22) or (3.23) that, at the above-mentioned point of the closing $C^-$-characteristic *fw*.

$$[\mu_1] = [\mu_2] = [\mu_3] = 0$$

Since, according to relations (3.24) and (3.25), discontinuities along characteristics do not disappear, then, despite the assumption which has been made, the solution of the conjugate problem cannot have discontinuous $C^0$- and $C^+$-characteristics arriving on *fw*.

The discontinuities along the streamlines on *fw* could arrive from the section $i_0w$ of the shock wave. Consequently, there cannot be points in $i_0w$ which generate such discontinuities. Discontinuous $C^+$-characteristics could arrive on *fw* or, more accurately, on the part of it *fc* from the generatrix $d_+f$. By virtue of the second condition of (3.13), a discontinuous $C^-$-characteristic could be reflected from $d_+f$. These characteristics arrive on $d_+f$ and, in particular, from the section $i^-w$ of the bow shock wave. Points of discontinuity, from which the emergence of discontinuous $C^-$-characteristics is permitted, can therefore only be located on the section $si^-$. We recall (Fig. 2b) that *s* is the point of arrival of the sonic line *dts* on the bow shock wave. Under the sonic line, the flow is subsonic and, in it, there are neither "discontinuous" nor "continuous" $C^+$- and $C^-$-characteristics, and only discontinuous $C^0$-characteristics, which are forbidden in the conjugate problem being considered, are possible. The multipliers under the sonic line are therefore continuous and, as a rule, they are finite on approaching *dts* from below. If., however, $\mu_k$ increase without limit at certain points of the sonic line, then it is natural to suppose that their increase in approaching these points along different "subsonic directions" for each $\mu_k$ occurs without a change of sign. We shall call the continuity of the magnitudes or (when they increase without limit) the signs of $\mu_k$ the "reflection condition". Hence, if a discontinuous $C^+$-characteristic arrives at the sonic line, it must be reflected by a discontinuous $C^-$-characteristic (and vice versa), ensuring that the reflection condition is satisfied at the point of reflection.

We will now investigate how the discontinuities in $\mu_k$ are reflected from the sonic line. On approaching the sonic line $\alpha \to \pi/2$, $\cos\alpha \to 0$ and, by virtue of formulae (3.25), we have

$$[\mu_2]^{\pm} \approx C_{\pm}\varepsilon, \quad [\mu_1]^{\pm} \approx \mp\frac{C_{\pm}(s\rho_s^{\circ} + \rho)}{\rho\varepsilon} V\sin\vartheta, \quad [\mu_3]^{\pm} \approx \pm\frac{C_{\pm}\rho_s^{\circ}}{\rho\varepsilon} V\sin\vartheta, \quad \varepsilon = \sqrt{\cos\alpha} \tag{3.27}$$

The plus (minus) superscripts indicate discontinuities in $\mu_k$ on discontinuous $C^+(C^-)$-characteristics, and $C^+$ and $C^-$ are constants determining the magnitude of the jumps in the incident and reflected discontinuities. If a discontinuous $C^+$-characteristic arrives at the sonic line, then the constant $C^+$ is known and $C^-$ is determined from the condition that there are no discontinuous $C^{\pm}$-characteristics in the subsonic flow domain. According to relations (32.7), the magnitude of the discontinuities in the multiplier $\mu_2$ tends to zero as the sonic line is approached, and $\mu_1$ and $\mu_3$ tend to infinity. In order to satisfy the reflection condition formulated above, at the points of reflection it is necessary that, with a chosen rule for calculating $[\mu_k]^{\pm}$ (for example, as the differences to the right and to the left of the discontinuous characteristics on moving along them towards the sonic line), the equality

$$C_- = C_+ \tag{3.28}$$

should be satisfied.

Discontinuous $C^-$-characteristics could arrive at the contour $d_+f$ not only from the section $i^-w$ of the bow shock wave but, also, from the section *dt* of the sonic line. This, however, is forbidden. Hence, if, together with the discontinuous $C^+$-characteristic *dw* in the bunch of rarefaction waves, there must also be other discontinuous $C^+$-characteristics by virtue of the conditions of the conjugate problem, then the only possibility is the characteristic *dt* which touches the sonic line. The other discontinuous characteristics of the bunch would generate discontinuous $C^-$-characteristics going to $d_+f$ as the result of reflection either from the section *dt* of the sonic line or, by virtue of condition (3.8) with a continuous Lagrange multiplier $\lambda(y)$ on the shock wave, from its section $i^+w$. The characteristic *dt* is special in this respect: at the point *t*, according to formulae (3.27) and (3.28), it "transfers" the discontinuity in $\mu_k$ going towards the shock wave to the section $ti^-$ of the $C^-$-characteristics. At the point $i^-$, the discontinuous $C^-$-characteristic is reflected by the discontinuous $C^+$-characteristic. That characteristic is reflected from the sonic line and so on, with bunching of the discontinuous $C^+$- and $C^-$-characteristics towards the point *s*.

In order to describe the reflection, from the bow shock wave, of the discontinuous $C^-$-characteristics, which, according to what has been said earlier, arrive at the section of the shock wave $si^-$, we use condition (3.18), which is satisfied on $i_0w$ and the continuity of the multiplier $\lambda(y)$ occurring in it. As in the case of reflection from the sonic line, we define $[\mu_k]^{\pm}$ as the differences to the right and to the left of the discontinuous $C^{\pm}$-characteristics as one moves along them towards the point where the bow shock wave is encountered. Having done the necessary calculations, we obtain

$$[\mu_1]^+ = k_1[\mu_1]^-, \quad [\mu_2]^+ = k_2[\mu_2]^-, \quad [\mu_3]^+ = k_3[\mu_3]^-, \quad k_1 = k_2\frac{\Phi_1^+}{\Phi_1^-}, \quad k_2 = \frac{\Phi_2^-}{\Phi_2^+}, \quad k_3 = k_2\frac{\Phi^+}{\Phi^-}$$

$$\Phi_1^\pm = sTa^{-2}\Phi^\pm\sin\alpha + \cos(\vartheta \mp \alpha), \quad \Phi_2^\pm = \rho_\infty u_\infty(u-u_\infty)\Phi^\pm - \rho V^2\sin\vartheta\sin^2\alpha \tag{3.29}$$

$$\Phi^\pm = \mp\{a^2\rho_p\sin\vartheta - \cos\alpha\sin(\vartheta \pm \alpha)\}, \quad \rho_p = \left(\frac{\partial\rho}{\partial p}\right)_i = \frac{\kappa}{a^2}, \quad sTa^{-2} = \frac{\ln(p\rho^{-\kappa})}{\kappa(\kappa-1)}$$

The expressions for $\rho_p$ and $sTa^{-2}$ are written for a perfect gas.

If the Lagrange multipliers satisfy the equation and conditions of the conjugate problem obtained above, then only variations of $x$ on $id$ and $d_+f$ and the increments in the coordinates of the point $d$ remain in the expression for $\delta\chi$, which enables one to obtain the necessary conditions for a minimum of $\chi$. Together with the expression for $\delta\chi$, they have the form

$$\delta\chi = Y\Delta y_d + X\Delta x_d + \left(\int_i^{d_-} + \int_{d_+}^{f}\right) B^x\delta^\circ x\,dy \tag{3.30}$$

$$Y \equiv \left\{ p_- - p_+ - (v\rho u)_+ + \int_{d_-}^{d_+} (\mu_1 + s\mu_3)d(\rho u) + \mu_2 d(p + \rho u^2) \right\}_d = 0$$

$$v = u - \mu_1 - s\mu_3$$

$$X \equiv \left\{ (v\rho v)_+ - (v\rho v)_- - \int_{d_-}^{d_+} (\mu_1 + s\mu_3)d(\rho v) + \mu_2 d(\rho u v) \right\}_d \geq 0 \tag{3.31}$$

$$B^x \equiv -y\rho v(\mu_1 + s\mu_3)' \geq 0 \quad \text{in} \quad id_- \tag{3.32}$$

$$B^x \equiv -y\rho v(\mu_1 + s\mu_3)' = 0 \quad \text{in} \quad d_+f \tag{3.33}$$

The equality (3.30) determines the optimum size of the front face. The equivalent numerical search for the minimum value of $C_x$ for fixed $l$ replaced it in the procedure for constructing short optimum bodies in Section 2. Inequalities (3.31) and (3.32), which correspond to the permissible variations of the abscissae of the corner points ($\Delta x_d \geq 0$) and of the front face $\delta x \geq 0$ when $0 \leq y \leq y_d$, are conditions for the fact that the front face is a section of a boundary extremum. Finally, equality (3.33), or

$$\mu_1 + s\mu_3 = \text{const} \tag{3.34}$$

is a necessary condition for an extremum, which determines the shape of the section $d_+f$. Hence, it follows from relations (3.10) and (3.13) that, on $d_+f$, all of the $\mu_k$ = const, $\mu_2 = -1$, and $\mu_1$ and $\mu_3$ are defined by equalities (3.26) written at the point $f$. The flow above the section $d_+f$ is supersonic. A change in its shape therefore has no effect on the flow past the front face (the generatrix $d_+f$ realizes a minimum of $\chi$ for a fixed front face). In the method of an undetermined control contour, this led to equality (1.3), which defines the parameters on the section $fc$ of the characteristic $fw$. On the optimum contour $d_+f$, the multipliers $\mu_k$ = const are known. Using them, from the solution of the Cauchy problem with the data in $d_+f$, we find $\mu_k$ in the triangle $d_+fc$, which includes the characteristic $fc$. We will show that (3.34) and the conditions of the conjugate problem in the triangle $d_+fc$ lead to condition (1.3).

We assume that the solution of the Cauchy problem in the triangle $d_+fc$ with $\mu_k$ = const in the contour $d_+f$ has the form

$$\mu_1 = \mu_1(\psi), \quad \mu_2 = -1, \quad \mu_3 = \mu_3(\psi) \tag{3.35}$$

In the triangle $d_+fc$, the initial system of equations (3.9) for $\mu_k$ is equivalent to the characteristic relations (3.10) and (3.12). On satisfying Eq. (3.10), the functions (3.35) reduce the two equations (3.12) to a single equation (a dot denotes a derivative with respect to $\psi$)

$$\dot{\mu}_1 + s\dot{\mu}_3 = 0 \tag{3.36}$$

In the triangle $d_+fc$, the entropy $s = s(\psi)$, and Eq. (3.36) is not at variance with a solution in the form of (3.35). At the same time, $\mu_1$ and $\mu_3$ satisfy relations (3.15) with $\mu_2 = -1$ on the section $fc$. It can be shown that substitution of $\mu_1$ and $\mu_2$, found from them, into Eq. (3.36) leads to the compatibility condition for the $C^-$-characteristics of the flow equation. Consequently, the functions $\mu_1(\psi)$ and $\mu_3(\psi)$, obtained from relations (3.15) with $\mu_2 = -1$, give the solution of the Cauchy problem in the triangle $d_+fc$, including the $C^+$-characteristic $d_+c$, and equality (1.3), which is obtained from (3.26) and (3.35), is satisfied on the section $fc$. Since, in the case of the generatrix $d_+f$, which satisfies the necessary conditions for an extremum, and, for any (not necessarily optimum) ordinate of the point $d$, the multipliers $\mu_k$ are known in the whole of the triangle $d^+cf$, it only remains to find the solution of the conjugate problem in the part of the domain $\Omega$ which lies to the left of the characteristic $d_+c$. Here, on the $C^+$-characteristic $d_+c$, the equalities (3.35), in which $\mu_1(\psi)$ and $\mu_3(\psi)$ are defined in the interval $fc$, are satisfied.

The flow past a short nose section constructed using the method described in Section 2 is known and, according to its construction, the gently sloping segment $d_+f$ satisfies the necessary condition for an extremum. Furthermore, the ordinate of the point $d$ also satisfies the necessary condition for an extremum. Hence, the solution of the conjugate problem is only necessary for verifying inequalities (3.31) and (3.32), that is, the necessary conditions for a minimum in $\chi$ which must be satisfied on the assumed section of the boundary extremum, the front face $id$. The conjugate problem is solved from right to left, that is, it starts from the supersonic domain where the method of characteristics can be used. Here, $\mu_k$ are known on the characteristics $d_+c$ and $wc$ and satisfy the final relation of (3.18) on the shock wave $i_0w$ with the continuous multiplier $\lambda(y)$, which is determined on $i_0w$ simultaneously with $\mu_k$ by solving problem (3.19) with the initial condition at the point $w$. On carrying out this solution mentally, it can be shown that, in the case of the nose shape which has been constructed, the conditions which have been enumerated uniquely define the finite $\mu_k$ up to the line $dti^-$, which consists of the section of the $C^+$- and $C^+$-characteristic $dt$ and $ti^-$ which are smoothly joined at the point $t$.

Under $dti^-$, the conjugate problem becomes an elliptic-parabolic (mixed) problem and the sections $dt$ and $ti^-$ may turn out to be lines of discontinuity of $\mu_k$ with all the consequences following from this, which have been described above. Using the finite values of $\mu_k$ found above $dti^-$, their values below this line (with $\mu_1$ and $\mu_2$ becoming infinite at the point $t$) are obtained by the addition of $[\mu_k]$. According to relations (3.25), (3.27) and (3.28), these values are given, apart from a previously unknown constant $C$, by the formulae

$$[\mu_1] = \pm C\frac{\cos(\vartheta \mp \alpha) + sTa^{-2}\Phi^{\pm}\sin\alpha}{\sqrt{y\rho}(M^2-1)^{1/4}\sin\vartheta\sin\alpha}, \quad [\mu_2] = \mp C\frac{(M^2-1)^{1/4}}{V\sqrt{y\rho}\sin\vartheta}$$

$$[\mu_3] = \mp C\frac{Ta^{-2}\Phi^{\pm}}{\sqrt{y\rho}(M^2-1)^{1/4}\sin\vartheta}$$

Here, $\Phi^{\pm}$ is the same as in (3.29) and the upper (lower) signs in front of $C$ and $\alpha$ and in the superscript refer to the section $dt/(ti^-)$ of the $C^+(C^-)$-characteristic.

## 4. CONCLUSION

The problem of constructing axisymmetric nose shapes with a specified aspect ratio $l$, that is, the ratio of their length to the radius of the base, which are optimum or close to optimum with respect to their wave drag, has been solved in the approximation of Euler's equations. For any aspect ratios, they have a front face, which is a section of a boundary extremum, that appears on account of the constraint on the maximum permissible length, and a gently sloping section which is joined to the front face with a corner point. Verification of the fact that the front face is a section of a boundary extremum is obtained using calculations of the flow past the bodies constructed and bodies which are obtained in the case of permissible deformation of the front face. An alternative method of proof, which does not assume the actual forms of variation of the front face, can be based on the solution of the conjugate problem within the framework of the generalized method of Lagrange multipliers. The formulation of this problem presented in Section 3 is of interest in its own right, in particular, on account of the previously unknown

features of the reflection of the discontinuities of Lagrange multipliers from the sonic line, with some of them becoming infinite.

Over the range of Mach numbers and aspect ratios $1.2 \leq M_\infty \leq 10$, $0.25 \leq l \leq 20$ investigated, the wave drag coefficients $C_x^N$ of the nose shapes constructed in the approximation of Newton's formula as well as of blunt nose shapes were greater than the drag coefficients $C_x$ of the optimum nose shapes constructed in the approximation of Euler's equations. However, when $M_\infty \geq 3.0$, the values of $C_x^N$ exceed the values of $C_x$ for nose shapes which are optimum in the approximation of Euler's equations, by just 0.8–9.4%. The reductions in their drag coefficients $C_x$, calculated within the framework of Euler's equations, compared with the values for cones, are found to be significantly greater than the analogous quantities determined using Newton's formula. This confirms the surprising efficiency of Newton's formula in problems of constructing the optimum configurations, but not when calculating their aerodynamic characteristics.

The optimum nose shapes constructed have smaller values of $C_x$ compared both with optimum blunt (single-parameter) and pointed (two-parameter) power law nose shapes. The first of these two types have been constructed earlier of $M_\infty \geq 2$ and $l \geq 1$.

The second type can only be successfully constructed for fairly large $l$: when $M_\infty \geq 3$ for $l \geq 4$ and, when $M_\infty = 1.5$ and 2, for $l \geq 6$. In the case of the above-mentioned $M_\infty$ and $l$, the excess of the values of $C_x^{m1}$ of the blunt, power-law nose shapes from [36] over the value of $C_x$ for the optimum nose shape is from 20% down to tenths of a percent, depending on $M_\infty \geq 2$. The pointed nose shapes constructed in [37] for $M_\infty = 1.5$ and $M_\infty = 2$ when $6 \leq l \leq 10$ and, for $M_\infty = 3$ and $M_\infty = 4$, when $4 \leq l \leq 10$ have values of $C_x^{m2}$ which exceed the values of $C_x$ for the optimum nose shapes by no more than 3.3%.

A calculation of the flow past optimum and blunt nose shapes with smooth contours for $M_\infty = 1.2$, $Re = 7 \times 10^6$ and $l = 4$, in the approximation of the Reynolds equations and the "$\nu_t$-90" model of turbulence,demonstrated the significant advantage of the optimum nose shapes both with respect to wave drag and overall drag.

We wish to thank I. A. Brailko for the program used to carry out the viscous flow calculations, S. A. Takovitskii for the results of calculations of pointed, power-law nose shapes and Yu. D. Shmyglevskii for useful remarks on the text of the manuscript.

This research was supported financially by the Russian Foundation for Basic Research (02-01-00422) and within the framework of the "State Support for the Leading Scientific Schools" programme (00-15-99039 and NSh-2124.2003.1).

## REFERENCES

1. NEWTON, I., *Mathematical Principles of Natural Philosophy* (translated from the Latin with a commentary by A. N. Krylov.). Nauka, Moscow, 1989.
2. NEWTON, I., *Mathematical Principles of Natural Philosophy* (*Philsophiae Naturalis Principia Mathematica*) (translated from the Latin by E. Motta, 1793; revised edition by F. Cajori). University of California Press, Berkeley, CA, 1947.
3. EGGERS, A. J. Jr., RESNIKOFF, M. M. and DENNIS, D. H., Bodies of revolution having minimum drag at high supersonic airspeeds. NACA Report, 1957, No. 1306.
4. EGGERS, A., Non-slender bodies of revolution of minimum wave drag. In *Theory of Optimal Aerodynamic Shapes* (edited by A. Miele). Mir, Moscow, 1969, 260–274.
5. KRAIKO, A. N., A Nose shape of specified volume, optimal with respect to wave drag in the approximation of Newton's drag law. *Prikl., Mat. Mekh.*, 1991, **55**, 3, 382–388. Also in *Gas Dynamics. Selection*, Vol. 1 (editor-author A. N. Kraiko). Fizmatlit, Moscow, 2000, 394–402.
6. GONOR, A. L. and CHERNYI, G. G., Bodies of minimum drag at high supersonic velocities. *Izv. Akad. Nauk SSR, Otd. Tekh. Nauk*, 1957, 7, 89–93.
7. GONOR, A. L., Determination of the shape of bodies of minimum drag at high supersonic velocities. *Prikl. Mat. Mekh.*,1960, **24**, 6, 1073–1078.
8. KRAIKO, A. N., The determination of bodies minimum drag using the Newton and Busemann drag laws. *Prikl. Mat. Mekh.*, 1963, **27**, 3, 484–495. Also in *Gas Dynamics. Selection*, Vol. 1 (editor-author A. N., Kraiko). Fizmatlit, Moscow, 2000, 381–393.
9. CHERNYI, G. G. and GONOR, A. L. Nonslender shapes of minimum pressure drag. *Theory of Optimum Aerodynamic Shapes* (edited by A. Miele). Academic Press, New York, 1965, 373–385.
10. KRAIKO, A. N., *Variational Problems of Gas Dynamics*. Nauka, Moscow, 1979.
11. KRAIKO, A. N., PUDOVIKOV, D. Ye. and YAKUNINA, G. Ye., *Theory of Aerodynamic Shapes Close to Optimal*. YaNUS-K, Moscow, 2001.
12. CHERNYI, G. G., Supersonic flow past a profile close to a wedge. In *Trudy TsIAM im. Baranova*, 1950, No. 197. Also in *Gas Dynamics. Selection*, Vol. 1 (editor-author A. N. Kraiko). Fizmatlit, Moscow, 2000, 443–462.
13. SHMYGLEVSKII, Yu. D., Supersonic profiles having minimum drag. *Prikl. Mat. Mekh.*, 1958, **22**, 2, 269–273.
14. SHMYGLEVSKII, Yu. D., A class of bodies of revolution with minimum wage drag. *Prikl. Mat. Mekh.*, 1960, **24**, 5, 923–926.
15. GUDERLEY, K. G., ARMITAGE, J. V. and VALENTINE, E. M., Nose and inlet shapes of minimum drag in supersonic flow. IAS Paper, 1962, 116.

16. SHMYGLEVSKII, Yu. D., *Some Variational Problems of Gas Dynamics*. Vychisl. Tsentr, Akad. Nauk SSSR, Moscow, 1963.
17. KRAIKO, A. N., *Variational Problems of Supersonic Gas Flows with Arbitrary Thermodynamic Properties*. Vychisl. Tsentr, Akad. Nauk SSSR, Moscow, 1963.
18. SHMYGLEVSKII, Yu. D., *Analytical Investigation of Fluid Dynamics*. Editorial URSS, Moscow, 1999.
19. BORISOV, V. M., The optimum shape of bodies in supersonic gas flow. *Zh. Vychisl. Mat. Mat. Fiz.*, 1963, **3**, 4, 788–793.
20. SHIPILIN, A. V., Optimum shapes of bodies with attached shock waves. *Izv. Akad. Nauk SSSR*. MZhG, 1966, 4, 9–18.
21. SHIPILIN, A. V., Variational problems of gas dynamics with attached shock waves. In *Collection of Theoretical Papers on Hydromechanics*. Vychisl. Tsentr, Akad. Nauk SSSR, Moscow, 1970, pp. 54–106.
22. KRAIKO, A. N. and SHELOMOVSKII, V. V., Nose shapes of bodies of revolution with a channel close to bodies of minimum wave drag. *Izv. Akad. Nauk SSSR. MZhG*, 1984, 1, 138–145.
23. KRAIKO, A. N. and PUDOVIKOV, D. Ye., The construction of the optimum contour of the nose section of a body in supersonic flow. *Prikl. Mat. Mekh.*, 1995, **59**, 3, 419–434. Also in *Gas Dynamics. Selection*, Vol. 1 (editor-author A. N. Kraiko). Fizmatlit, Moscow, 2000, 463–480.
24. GONOR, A. L. and KRAIKO, A. N., Some results of an investigation of optimum shapes at supersonic and hypersonic velocities. In *Theory of Optimum Aerodynamic Shapes* (edited by A. Miele). Mir, Moscow, 1969, 455–492.
25. KRAIKO, A. N., Variational problems of gas dynamics, formulations, methods of solution, correlation of exact and approximate approaches. In *Problems of Contemporary Mechanics*, Part I (edited by L. I. Sedov). Izd. MGU, Moscow, 1983, 90–100.
26. KRAIKO, A. N. and P'YANKOV, K. S., Design of profiles and engine nacelles, supercritical in a transonic flow of a perfect gas. *Zh. Vychisl. Mat. Mat. Fiz.*, 2000, **40**, 12, 1890–1904. Also in *Gas Dynamics. Selection*, Vol. 2 (editors-authors A. N. Kraiko, A. B. Vatazhin and A. N. Sekundov). Firzmatlit, Moscow, 2001, 250–264.
27. KRAIKO, A. N., P'YANKOV, K. S. and TILLYAYEVA, N. I., Profiling of the supersonic section of a plate-like jet in a non-uniform transonic flow. *Izv. Ross. Akad. Nauk. MZhG*, 2002, 4, 145–157.
28. KRAIKO, A. N., MYSHENKOV, Ye. V., P'YANKOV, K. S. and TILLYAYEVA, N. I., Effect of non-ideality of a gas on the characteristics of a Laval nozzle with an abrupt constriction. *Izv. Ross. Akad. Nauk. MZhG*, 2002, 5, 191–204.
29. GODUNOV, S. K., ZABRODIN, A. V., IVANOV, M. Ya. *et al.*, *Numerical Solution of Multidimensional Problems of Gas Dynamics*. Nauka, Moscow, 1976.
30. KOLGAN, V. P., The use of the principle of minimum values of a derivative to construct finite difference schemes for calculating discontinuous solutions in gas dynamics. *Uch. Zap. TsAGI*, 1972, **3**, 6, 68–77.
31. RODIONOV, A. V., A monotonic second order of approximation scheme for the direct calculation of non-equilibrium flows. *Zh. Vychisl. Mat. Mat. Fiz.*, 1987, **27**, 4, 585–593.
32. RODIONOV, A. V., Increasing the order of approximation of S. K. Godunov's scheme. *Zh. Vychisl. Mat. Mat. Fiz.*, 1987, **27**, 12, 1853–1860.
33. TILLYAYEVA, N. I., Extension of the modified S. K. Godunov scheme to arbitrary non-regular meshes, *Uch. Zap. TsAGI*, 1986, **17**, 2, 18–26. Also in *Gas Dynamics. Selection*, Vol. 2 (editors-authors A. N. Kraiko, A. B. Vatazhin and A. N. Sekundov). Firzmatlit, Moscow, 2001, 201–210.
34. KRAIKO, A. N., MAKAROV, V. Ye. and TILLYAYEVA, N. I., The numerical construction of shock wave fronts. *Zh. Vychisl. Mat. Mat. Fiz.*, 1980, **20**, 3, 716–723. Also in *Gas Dynamics. Selection*, Vol. 2 (editors-authors A. N. Kraiko, A. B. Vatazhin and A. N. Sekundov). Fizmatlit, Moscow, 2000, 169–175.
35. CHERNYI, G. G., *Gas Dynamics*. Nauka, Moscow, 1988.
36. GRODZOVSKII, G. L. (Ed.), *Aeromechanics of Supersonic Flow Part Bodies of Revolution of Power-Law Form*. Mashinostroyeniye, Moscow, 1975.
37. TAKOVITSKII, S. A., Pointed two-parameter power-law nose shapes of minimum wave drag. *Prikl. Mat. Mekh.*, 2003, **67**, 5, 829–835.
38. KRAIKO, A. N., and PUDOVIKOV, D. Ye., The role of a constraint of length in the construction of bodies of minimum drag. *Prikl. Mat. Mekh.*, 1997, **61**, 5, 822–837. Also in *Gas Dynamics. Selection*, Vol. 1 (editor-author A. N. Kraiko). Fizmatlit, Moscow, 2000, 493–511.
39. KRAIKO, A. N., and PUDIVIKOV, D. Ye., The design of symmetric profiles, optimum in supersonic and hypersonic flow under arbitrary isoperimetric conditions. *Prikl. Mat. Mekh.*, 1997, **61**, 6, 931–946.
40. KOZLOV, V. Ye., SEKUNDOV, A. N. and SMIRNOVA, I. P., Models of turbulence for describing the flow in a jet of a compressible gas. *Izv. Akad. Nauk SSSR. MZhG*, 1986, **6**, 38–44.
41. GULYAYEV, A. N., KOZLOV, V. Ye. and SEKUNDOV, A. N., The construction of a universal one-parameter model for turbulent viscosity. *Izv. Ross. Akad. Nauk. MZhG*, 1993, 4, 69–81. Also in *Gas Dynamics. Selection*, Vol. 2 (editors-authors A. N. Kraiko, A. B. Vatazhin and A. N. Sekundov). Fizmatlit, Moscow, 2001, 440–454.
42. KOPCHENOV, V. I., LOMKOV, K. E. and TOPEKHA, Ye. A., Methods and results of a calculation of the flows of a viscous gas in channels and jets. *Annotated Proceedings of the 7th All-Union Congress on Theoretical and Applied Mechanics*. Izd. Akad. Nauk SSSR, Moscow, 1992, 200.
43 GOUSKOY, O. V., KOPCHENOV, V. I. and NIKIFOROV, D. A., Flow numerical simulation in the propulsion elements of aviation space system within full Navier–Stokes equations. *Proc. 7th Intern. Conf. Methods of Aerophysical Research*, Part 1. Novosibirsk, 1994, 104–109.
44. BRAILKO, I. A. and KLESTOV, Yu. M., Mathematical modelling and experimental investigation of the gas dynamic characteristics of a "planar" nozzle. *Annotated Proceedings of the 8th All-Russian Congress on Theoretical and Applied Mechanics*. Inst. Mekh. Sploshnykh Sred, UrO Russ. Akad. Nauk, Perm, 2001, 119.
45. VYSHINSKII, V. V. and KUZNETSOV, Ye. N., Allowance for friction when choosing of the optimum shapes of nose sections of bodies of revolution in sonic flow. *Uch. Zap. TsAGI*, 1986, **17**, 3, 110–144.
46. VYSHINSKII, V. V., KUZNETSOV, Ye. N. and MIKHAILOV, P. D., Optimum shapes of the nose sections of bodies of revolution in transonic flow. *Uch Zap. TsAGI*, 1988, **19**, 6, 103–105.

*Translated by* E.L.S.